Appendix A

Materials Degradation Modes and their Prediction

"He that will not apply new remedies must expect new evils; for time is a great innovator," from *Essays II Of Innovations,* Sir Francis Bacon (1561-1626)

"No sooner knew the reason, but they sought the remedy," from *As You Like It,* Shakespeare (1564-1616)

A.1 Introduction

In order to satisfy the objective of this Proactive Material Degradation Assessment it is necessary that, as Sir Francis Bacon and Shakespeare recognized, the various modes of degradation (e.g. stress corrosion cracking, crevice corrosion, thermal embrittlement, etc.) be defined and, in order to be proactive, there should be quantitative life-prediction capabilities for each of them. Some of the challenges to having an adequate prediction capability were discussed in Section 2.4, with examples taken specifically for the case of stress corrosion. In this Appendix, a wider range of materials degradation modes are described, together with a brief description of the mechanisms and system parameters that control the extent of degradation. This information serves as an introduction to more extensive discussions in the topical reports given in Appendix B, which present the rationale for the panelists' susceptibility, confidence and knowledge scoring of degradation in various Light Water Reactor (LWR) systems. The degradation modes considered in this Appendix are:

- General corrosion, including boric acid corrosion and flow-accelerated corrosion.
- Localized corrosion, including crevice corrosion, pitting, galvanic attack, microbiologically influenced corrosion, and various modes of stress corrosion.
- Fatigue, including corrosion fatigue.
- Embrittlement, including that associated with fast neutron exposure, thermal aging and hydrogen embrittlement.

Since many of these degradation modes involve corrosion, a brief primer is included on corrosion basics, so as to orientate the reader to phraseology and concepts.

A.2 Materials of Construction

As detailed in Tables A.1-A.4 there is a large variety of metallic materials used in the fabrication of PWR and BWR pressure boundary and internal components, including:

1. *Reactor Coolant Piping and Fittings* – carbon steel, low-alloy steel, cast and wrought stainless steels and various weld materials depending on the parent material used.
2. *Reactor Pressure Vessel* and *PWR Pressurizer Vessel* - low-alloy steel, stainless steel cladding, wrought nickel-based penetrations and various weld materials depending on the components being joined.
3. *Reactor Internals* – cast and wrought austenitic stainless steels, nickel-based alloys, and their associated weld metals.
4. *PWR Steam Generator* – low alloy and carbon steels, stainless steel cladding, nickel-base alloys, and various weld materials depending on the components being joined.
5. *Pumps* – cast and wrought austenitic stainless steels for pressure boundary materials; various high alloy steels for bolting and austenitic or martensitic stainless steels for pump shafts and other internal components.

Table A. 1 Materials in Carbon & Low Alloy Steels Used in LWR Pressure Vessels & Piping (wt. %) [ ]

	A533-B	A508-2	A508-3	A333-6	A516
Carbon	≤0.25	≤0.27	≤0.25	≤0.30	≤0.28
Manganese	1.15 – 1.50	0.5 – 1.00	1.20 – 1.50	0.29- 1.06	0.60 – 1.20
Phosphorus	≤0.035	≤0.025	≤0.025	≤0.025	≤0.035
Sulfur	≤0.035	≤0.025	≤0.025	≤0.025	≤0.035
Silicon	0.15 – 0.40	0.15 – 0.40	0.15 – 0.40	≤0.10	0.15 – 0.40
Nickel	0.40 – 0.70	0.50 – 1.00	0.40 – 1.00		
Chromium		0.25 – 0.45	≤0.25		
Molybdenum	0.45 – 0.60	0.55 – 0.70	0.45 – 0.60		
Vanadium		≤0.05	≤0.05		

Table A. 2 Materials in Some Stainless Steels Commonly Used in LWRs (wt. %) [ ]

	Type 304L	Type 316	Type 321	Type 347	Type 308L	Type 309L	A-286	17-4PH
Carbon								
Manganese	≤2.0	≤2.0	≤2.0	≤2.0	≤2.0	≤2.0	≤2.0	≤1.00
Silicon	≤1.0	≤1.0	≤1.0	≤1.0	≤1.0	≤1.0	≤1.0	≤1.00
Chromium	18-20	16-18	17-19	17-19	19-21	22-24	12-15	15-17.5
Nickel	8-12	10-14	9-12	9-13	10-12	12-15	24-27	3.0-5.0
Molybdenum		2.0-3.0					1.00-1.50	
Phosphorus	≤0.045	≤0.045	≤0.045	≤0.045	≤0.045	≤0.045	≤0.040	≤0.040
Sulfur	≤0.030	≤0.030	≤0.030	≤0.030	≤0.030	≤0.030	≤0.030	≤0.030
Other elements			Ti >5C	Nb+Ta >10C			Ti 1.55-2.00 Al ≤0.35 V 0.10-0.50	Cu 3.0-5.0 Nb+Ta 0.15-0.45

Table A. 3 Materials in Cast Stainless Steels used in LWRs (wt. %) [ ]

	CF-3	CF-3A	CF-8	CF-8A	CF-8M
Carbon %min	0.03	0.03	0.08	0.08	0.08
Manganese %min	1.50	1.50	1.50	1.50	1.50
Silicon %min	2.00	2.00	2.00	2.00	1.50
Sulfur %min	0.040	0.040	0.040	0.040	0.040
Phosphorus %min	0.040	0.040	0.040	0.040	0.040
Chromium	17.0-21.0	17.0-21.0	18.0-21.0	18.0-21.0	18.0-21.0
Nickel	8.0-12.0	8.0-12.0	8.0-11.0	8.0-11.0	9.0-12.0
Molybdenum %min	0.50	0.50	0.50	0.50	2.0-3.0

All of the above materials are potentially susceptible to one or more degradation modes, depending upon the combinations of material and service conditions. Some of these combinations are indicated in Table A.5.

Alloys, which may potentially degrade by a given mode in a given system, are shaded in Table A.5 (with no judgment being made as to the extent of the degradation). The environmental conditions shown in the table have been chosen to represent the range of chemistry and temperature conditions in various PWR systems (e.g. Reactor Coolant System, both primary and secondary; Emergency Core Coolant System (ECCS); Service Water; etc). Although stress corrosion and fatigue are possible for the majority of the chosen environment/material combinations, other degradation modes will change with different system conditions. For instance, microbiologically-induced-corrosion (MIC) will not be an issue in the higher temperature borated RCS, since the microbes cannot survive under these conditions, but MIC may be an issue in the lower temperature systems, such as parts of the ECCS, and especially in those reactor systems that are not borated, such as the component coolant and service water systems. Ranges in temperature are shown in some of the system examples, and this will give rise to a range in degradation susceptibilities within that system since most of the degradation modes are temperature activated. It is the objective of the PMDA project to assess the degree to which these susceptibilities may vary due to temperature, material condition, etc. for each component within the various subsystems (and whether there is sufficient knowledge to predict and mitigate this damage). It should also be noted in Table A.5 that many of the alloy/degradation mode combinations are shown blank, indicating that although there may be a possibility of degradation, its likelihood of occurring is small. The rationale for such judgments is either the fact that that particular combination (marked with an X) does not occur (e.g. there are no Alloy 82/182 welds in the highly irradiated core region, so irradiation induced creep is

unlikely), or there are mechanistic reasons to judge that the likelihood of degradation is low; this latter aspect is covered in Section A.4 of this Appendix.

Table A.4 Materials in Nickel base alloys used in LWRs (wt. %) [ ]

	Alloy 600	Alloy 182	Alloy 82	Alloy 690	Alloy 152	Alloy 52	Alloy 800	Alloy X750	Alloy 718
Nickel	>72.0	Bal.	Bal.	>58.0	Bal.	Bal.	30-35	>70.0	50-55
Chromium	14-17	13-17	18-22	28-31	28-31.5	28-31.5	19-23	14-17	17-21
Iron	6-10	≤10.0	≤3.00	7-11	8-12	8-12	>39.5	5-9	Bal.
Titanium		≤1.0	≤0.75		≤0.50	≤1.0	0.15-0.60	2.25-2.75	0.65-1.15
Aluminum						≤1.10	0.15-0.60	0.4-1.0	0.2-0.8
Niobium plus Tantalum		1.0-2.5	2.0-3.0		1.2-2.2	≤0.10		0.7-1.2	4.75-5.50
Molybdenum					≤0.50	≤0.05			2.8-3.3
Carbon	≤0.05	≤0.10	≤0.10	≤0.04	≤0.045	≤0.040	≤0.10	≤0.08	≤0.08
Manganese	≤1.0	5.0-9.5	2.5-3.5	≤0.50	≤5.0	≤1.0	≤1.50	≤1.0	≤0.35
Sulfur	≤0.015	≤0.015	≤0.015	≤0.015	≤0.008	≤0.008	≤0.015	≤0.010	≤0.010
Phosphorus		≤0.030	≤0.030		≤0.020	≤0.020			
Silicon	≤0.5	≤1.0	≤0.50	≤0.50	≤0.65	≤0.50	≤1.0	≤0.5	≤0.35
Copper	≤0.5	≤0.50	≤0.50	≤0.5	≤0.50	≤0.30	≤0.75	≤0.5	≤0.30
Cobalt	≤0.10	≤0.12	≤0.10	≤0.10	≤0.020	≤0.020			

Table A.5 Expected Alloy/Degradation Mode Combinations for PWRs
(GC=General Corrosion; BAC=Boric Acid Corrosion; FAC= Flow Accelerated Corrosion; CREV= Crevice Corrosion; PIT=Pitting; GALV=Galvanic Attack; SCC=Stress Corrosion Cracking; MIC= Microbiologically-Induced Corrosion; FAT=Fatigue)

	"General Corrosion"			"Localized Corrosion"					"Mechanical"			
Alloy System	GC	BAC	FAC	CREV	PIT	GALV	SCC	MIC	FAT	Therm. Emb.	Irrad Emb	Irrad Creep
	Reactor Coolant System, 550-650 F, PWR Primary and Secondary Water											
Low Alloy & Carbon Steel												
Wrought Stainless Steel, 304/316												
Stainless Steel Welds 308/309												
Cast Stainless Steel CF8/CF8M											X	X
Alloy 600 Nozzles, Safe-ends, SGTubes											X	X
Alloy 82/182 Welds											X	X
	Main Feedwater, 250-450F, Demin Water, pH 9-10											
Carbon Steel Piping												
Alloy 690 Forging												
	Main Steam Line, 445-530F , Steam											
Low Alloy & Carbon Steel												
	CVCS, 115-290F, PWR Primary Water											
Low Alloy Steel Bolts (assume leakage)												
Wrought Stainless Steel, 304/316												
Stainless Steel Welds 308/309												
Cast Stainless Steel CF8/CF8M												
	Emergency Core Cooling System, 100-150 F, Borated Demin Water											
Wrought Stainless Steel, 304/316												
Stainless Steel Welds 308/309												
Cast Stainless Steel CF8/CF8M												
	Component Cooling Water,105-130F, Treated Water											
Low Alloy & Carbon-Steel Piping / Fittings												
	Service Water System, 100F, Pond Water											
Low Alloy & Carbon-Steel Piping / Fittings												
Wrought Stainless Steel, 304/316 HX tubing												
Stainless Steel Welds 308/309												
Copper base alloys HX tubing												

A.3 Corrosion Basics

Corrosion of metals in aqueous environments involves various electrochemical and chemical reactions at, or close to, the material/environment interface. For instance simplified reaction equations may be formulated for the electrochemical oxidation of a metal atom to form either (a), a solvated metal cation (Equation A.1) or (b), in alkaline solutions, a metal anion (Equation A.2); or,(c) an oxide may be formed directly on the surface (Equation A.3) by electron transfer. Alternatively, the oxide may also form adjacent to, and then deposit onto, the surface via a precipitation reaction (Equation A.4).

$$M + H_2O \rightarrow M_{aq}^{z+} + ze^- \qquad \text{A.1}$$

$$M + n\,H_2O \rightarrow MO_n^{n-} + 2nH^+ + ne^- \qquad \text{A.2}$$

$$M + H_2O \rightarrow MO + 2\,H_2O + 2e^- \qquad \text{A.3}$$

$$M_{aq}^{z+} + H_2O \rightarrow MO + H+ \qquad \text{A.4}$$

Detailed research and development has focused on the kinetics and thermodynamics of such reactions since they are central to the development of corrosion mitigation actions used in numerous industries; such actions include, for instance, anodic and cathodic protection, development of various inhibitors and paint schemes, alloy development, water chemistry control, etc. Discussion of such developments and the science behind them is outside the scope of this present discussion, and the reader is directed towards appropriate textbooks, such as References 1-6, for such details.

Under equilibrium conditions the change in Gibbs free energy, ΔG, associated with those surface reactions involving electron transfer (Equations A.1-A.3) will have a related electrode potential, E, at that surface (Equation A.5) with the value of that potential being a function of temperature, metal cation or anion activity (for Equations A.1 and A.2) and pH (for Equations A.2 and A.3).

$$E = -\Delta G/zF \qquad \text{A.5}$$

where F is Faradays constant (96,500 coulombs/equivalent), and z is the number of electrons (or equivalents) exchanged in the reaction.

Again the reader is referred to corrosion texts [1-6] for details of these electron transfer relationships, and the derivation of the electrode potential that exists at the metal/solution interface. The equilibrium stability of the precipitated oxide in Equation A.4 will be dependent on the interactions between temperature, pH and oxide solubility. These fairly basic concepts lead to the construction of a Pourbaix diagram [7], which denotes the potential/pH combinations where various species (M, MO, M_{aq}^{z+}, MO_n^{n-}) are thermodynamically stable or metastable at a given temperature.

Such diagrams are of extreme value in predicting corrosion events and in determining E/pH combinations where the metal is, (a) thermodynamically immune from corrosion or, (b) where it is possible that the surface may be protected by an oxide (or salt) which may, depending on its structure, confer "passivity" or, (c) where the metal may undergo active corrosion. With this knowledge, mitigation strategies associated with, for instance, water chemistry specifications or alloy choice can be formulated.

Such a Pourbaix diagram for the iron-water system, at 25°C and activities of dissolved species of 10^{-6} gm-equivalents/L, is shown in Figure A.1. It is seen that, at lower potentials, there is a region in potential-pH space where the oxidation Equations A.1-A.3 are not possible thermodynamically, and iron is immune from corrosion. However, corrosion is possible at more positive potentials corresponding to the general oxidation Equations A.1 and A.2 where the dissolved species are Fe^{2+} or Fe^{3+} in acid conditions and $HFeO_2^-$ in alkaline solutions.

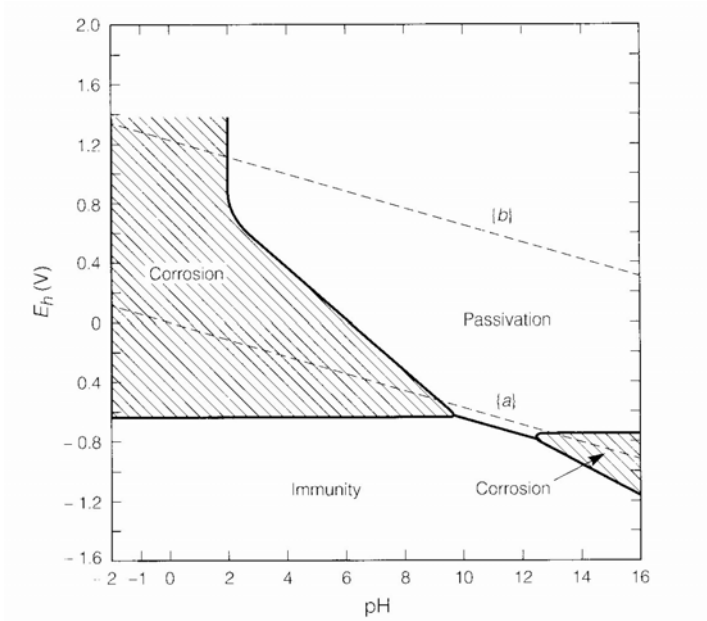

Figure A.1 Pourbaix diagram for the iron- water system at 25°C, Activities of dissolved species of 10^{-6} gm-equivalents/L [7]

Oxides (Fe_3O_4, Fe_2O_3) are stable at intermediate pH values via oxidation reactions (Equation A.3) or dissolution/ precipitation reactions (Equation A.4) and may, depending on the oxide structure confer corrosion protection via "passivity". Alloying may significantly affect the oxide structure and the degree of passivation, which is conferred at various E/pH conditions. A simple example of this is shown in Figure A.2 where the stability region for Cr_2O_3 is superimposed onto the Pourbaix diagram for the iron-water system. It is seen that the passivity region is considerably expanded, with the potential for improved corrosion resistance with ferritic stainless steels (Fe-Cr alloys) and austenitic stainless steels (Fe-Cr-Ni) due to the formation of mixed spinel oxides on the metal surface. Again the reader is guided to the corrosion handbooks that refer to numerous papers that focus on the details of these phenomena.

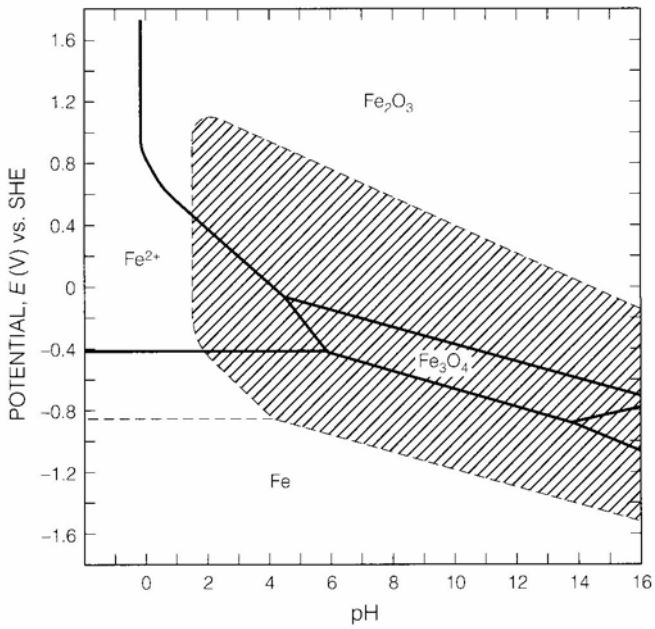

Figure A.2 Superimposition of $Cr(OH)_{32}O_3$ stability region onto the Pourbaix diagram for the iron-water system at 25°C and activities of dissolved species of 10^{-6} gm-equivalents/L. [4; adapted from 7].
Note that the alternate Cr_2O_3 phase has a similar outline but with reduced stability regions in the acid and alkaline regions.

Pourbaix diagrams may be also used for the prediction of corrosion degradation modes other than general corrosion, since many of these are dependent on the conjunction of reactions such as Equations A.1- A.4. Such a use is discussed in Appendix B relative to the E/pH combinations known to be relevant for various submodes of stress corrosion cracking of nickel-base alloys in PWR steam generators [see Appendix B.7].

Finally, in discussing the thermodynamics of the various species at the metal – environment interface, it is important to point out that the Pourbaix diagram sets bounds on the kinetics of formation of those species. For example, metal dissolution via Equation A.1, cannot occur, even at extremely slow rates at potentials more negative than the reversible potential for that reaction. The rate of dissolution at potentials above the reversible potential will depend on various factors that are now discussed.

The extent of corrosion, or the mass of metal oxidized per unit area, is equivalent Faradaically to the oxidation charge density passed in Equations A.1-A.3. However, in order to conserve charge under open circuit conditions (i.e the metal does not have an imposed current on it as would be the case with anodic or cathodic protection), the release of electrons in such oxidation reactions must be balanced by an equal consumption of electrons by reduction reactions. In LWRs such reactions commonly involve reduction of hydrogen cations (Equation A.6), water (Equation A.7) or dissolved oxygen (Equation A.8), or may be associated with other reactions associated with reduction of hydrogen peroxide, cupric cations, etc.

$$2H^+ + 2e \rightarrow H_2 \qquad \text{A.6}$$

in acid solutions or, in neutral or alkaline solutions

$$2H_2O + 2e^- \rightarrow H_2 + 2OH^- \qquad \text{A.7}$$

and

$$O_2 + 2H_2O + 4e^- \rightarrow 4OH^- \qquad \text{A.8}$$

The fact that reduction reactions must also occur on the metal surface has an impact on the regimes on the Pourbaix diagram that are applicable for a given system. For instance, Equation A.6 is an appropriate reduction process in deaerated water, and the line "a" in Figure A.1 indicates the equilibrium potential/pH relationship. Thus, in order to have reduction according to Equation A.6 in conjunction with oxidation of iron by Equations A.1-A.3, the relevant potential/pH area lies below line "a". By contrast in aerated water, where a relevant reduction reaction would be Equation A.8 (whose equilibrium potential / pH relationship is given by line "b" in Figure A.1), the relevant potential/pH area on the Pourbaix diagram is considerably increased. Thus there is a thermodynamic reason why, in general, corrosion problems are potentially more significant in aerated vs dearated solutions.

As shown schematically in Figure A.3 the oxidation and reduction reactions may take place on adjacent areas of the material surface, but this is not always the case, especially for localized corrosion modes when the "anodic" and "cathodic" sites (where the oxidation and reduction reactions respectively occur) may be separated for geometric or metallurgical inhomogeniety reasons.

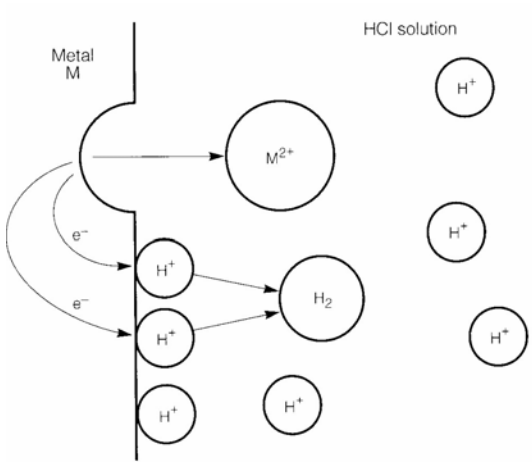

Figure A.3. Oxidation and reduction reactions occurring on adjacent areas of surface [4]

The kinetics of the oxidation and reduction reactions for the simple case of zinc dissolving in an acid solution are shown in Figure A.4 in order to illustrate the concept of the equilibration of

oxidation and reduction reaction rates. It is seen that the oxidation, or dissolution, rate for zinc, quantified by the current density for the reaction,

$$Zn \rightarrow Zn^{2+} + 2e^{-}$$

increases exponentially with the extent that the surface potential is increased from the potential associated with equilibrium for that reaction; this difference between the equilibrium potential and the surface potential is known as the overpotential. Similarly the reduction rate for hydrogen cations for the reaction occurring on the adjacent metal surface also increases exponentially with increasing overpotential for that reaction. At a surface potential denoted as the corrosion potential, E_{corr}, the rate of oxidation equals the rate of reduction, and the zinc corrosion rate is defined by the corrosion current density, i_{corr} (Note that in terminology generally used in corrosion in nuclear systems, E_{corr} is usually termed the electrochemical corrosion potential, or ECP).

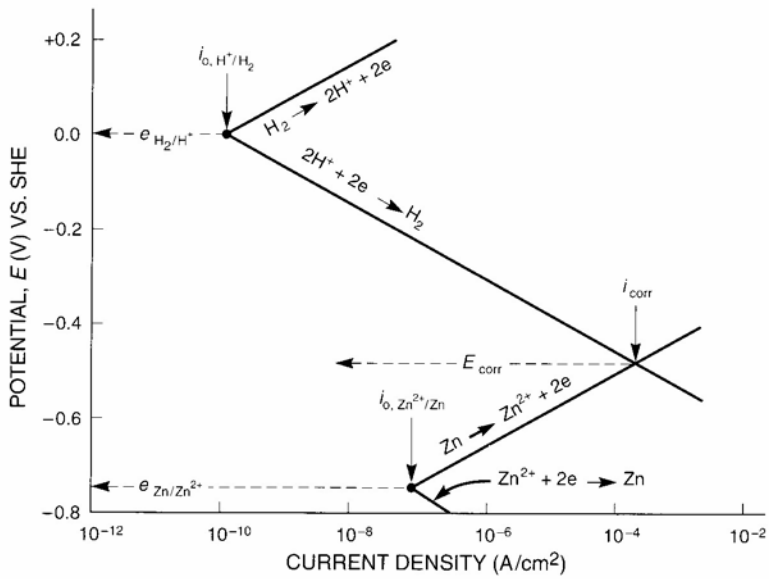

Figure A.4 Schematic "Evans" diagram indicating the equilibration of the oxidation and reduction rates for the dissolution of zinc in 1N HCl solution, and the associated "corrosion current, (i_{corr})" and "corrosion potential, (E_{corr})" [6]

This simple kinetic system may become more complicated when, as mentioned above, the "anodic" and "cathodic" sites are separated for geometric or metallurgical inhomogeniety reasons or where the areas on the metal surface associated with oxidation and reduction reactions are markedly different. These are particularly important in localized corrosion events, and will be discussed later in the appropriate section.

In order to control corrosion product (or "crud") release in the reactor coolant system, alloys are used that operate in the region of the Pourbaix diagram where surface protection is provided by the presence of a protective oxide film. The effect of the formation of such a film on the kinetics

of oxidation is shown schematically in Figure A.5. As the overpotential for oxidation is increased so the corrosion rate may increase exponentially under "activation control" until a potential, predictable from the Pourbaix diagram, is reached when an oxide may form. Thereupon the oxidation rate decreases by a factor of 10^4 or more dependent on the structure, composition and solubility of the oxide. The increased corrosion resistance may be maintained over a considerable potential range until, at more positive potentials, the oxide may lose it's protective properties, either due to the onset of localized breakdown due to the presence of aggressive impurity anions (such as chloride) leading to pitting [see Appendix B.9, 8] or, in extreme conditions, to Cr_2O_3 -rich oxide dissolution to e.g. $HCrO_4^-$.

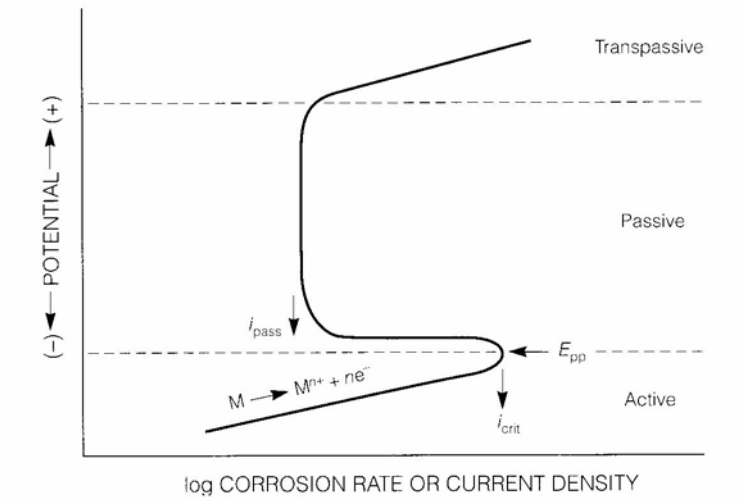

Figure A.5 Schematic oxidation current density vs. electrode potential diagrams, indicating, for the oxidation reactions, transitions from activation control, to onset of passivation, to oxide break down due to transpassivity or pitting. [4]

The prediction of the kinetics of corrosion reactions is further complicated by the fact that many of the oxidation and reduction reactions occurring on the metal surface may be ultimately controlled by the transport of either reaction products away from the surface, or by the transport of reactants to the metal surface. This is especially the case for material geometries, which are constricted, such as crevices and cracks; these situations will be discussed in the appropriate sections on localized corrosion later in this Appendix and in the topical reports in Appendix B. An example of such a complication due to mass transport under general corrosion conditions is shown schematically in Figure A.6 where the kinetics for the reduction of dissolved oxygen are superimposed on the metal oxidation kinetics from Figure A.5. In this situation it is seen that the "activation controlled" reduction kinetics increase exponentially with overpotential to a limiting value when the reduction rates become potential-independent. This limitation corresponds physically to the point when dissolved oxygen cannot arrive fast enough to the reacting surface to satisfy any further increase in activation controlled processes. As would be expected, however, this condition is delayed if the bulk-dissolved oxygen content is increased or if the solution flow rate is increased; both of these actions effectively increase the concentration of oxygen and reduction kinetics at the reacting metal surface. It is apparent that the corrosion current density and corrosion potential can change in a non-monotonic manner with different

changing system conditions, but these can be predicted via knowledge of the oxidation rates and the reduction rates associated, in this example, with dissolved oxygen content, solution flow rate, etc.

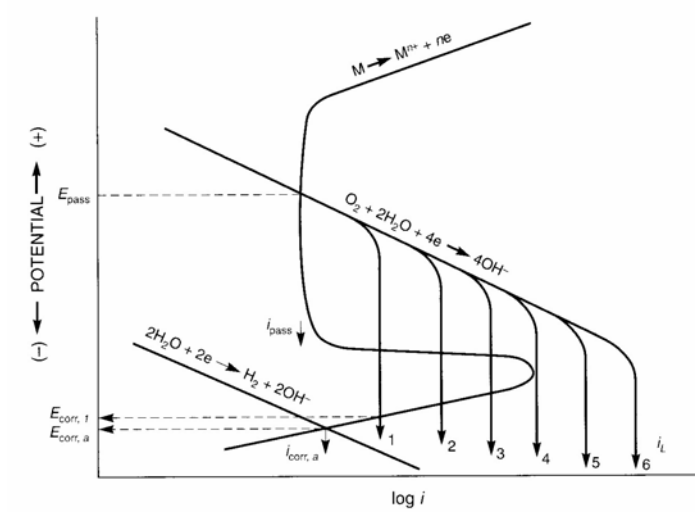

Figure A.6 Superposition of the reduction kinetics for dissolved oxygen on the metal oxidation rates from Figure A.5. In this case the reduction kinetics may be limited by the supply of oxygen to the reacting surface. [4]

A.4 Description of Degradation Modes and their Predictability in LWRs

A.4.1 "General" Corrosion

This section addresses degradation mechanisms, which result in loss of material over a reasonably large area (as opposed to localized corrosion that occurs over areas of less than 1-2 cm^2). Such degradation modes include general corrosion, boric acid corrosion and flow accelerated corrosion.

General Corrosion

General corrosion is characterized by uniform surface loss through material oxidation (i.e., general Equations A.1- A.3), and is deleterious to plant operation due to (a) loss of functionality of a pressure boundary due to loss of section thickness, (b) the presence of corrosion products ("crud") which may decrease the heat transfer efficiency upon depositing on e.g. steam generator tubes or fuel cladding, and (c) the presence of crud which is deposited and activated on the fuel cladding surface and, upon release, will increase the radioactivity levels in the RCS or, in the case of direct cycle BWRs, the balance of plant.

General corrosion issues are part of the design basis of the LWRs and are founded on a large body of research over many decades. Thus there is good reason for the judgments in Table A.5 that general corrosion is a manageable issue in LWRs. The following discussion is included, however, since the electrochemical details of general corrosion in LWRs forms a basis for

understanding other corrosion-based degradation modes for which there may be less confidence in our ability to adequately manage the situation.

As explained in Section A.3 the corrosion rates may be managed by consideration of the thermodynamically stable (or metastable) species (dissolved metal cations, oxides, salts, etc.) at the metal / water interface and the control of the relevant oxidation and reduction kinetics. In the case of the main materials of construction in LWRs importance is attached to the surface oxide solubility, which, as indicated in Figure A.7, for magnetite in the iron/water system at 300^0C, exhibits a minimum at neutral or slightly alkaline conditions [9]. Very similar solubility /pH relationships are noted for chromium and nickel. Also shown in Figure A.7 is the dependency of the corrosion rate for mild steel on pH, which mirrors the oxide solubility dependency.

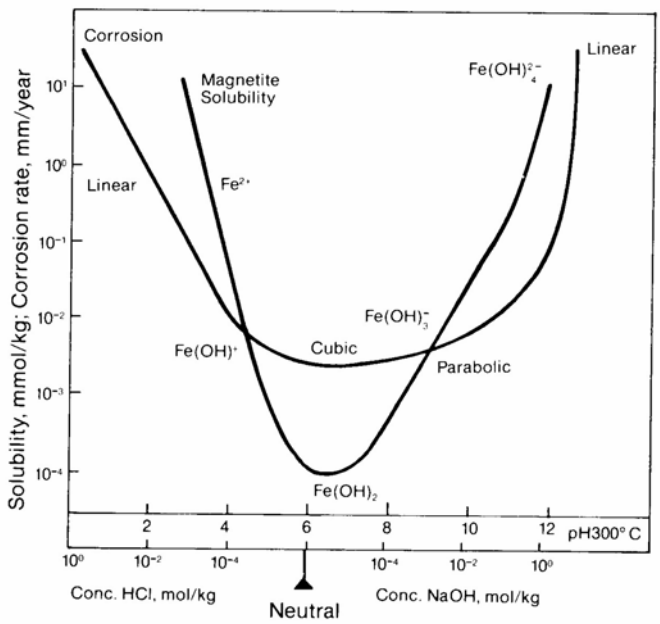

Figure A.7 Corrosion of mild steel and solubility of magnetite at 300^oC showing corrosion rate laws [11]

As explained in Section A.3 the corrosion rates of stainless steels and nickel-base alloys in high temperature water are significantly lower than those of carbon steels due to spinel type oxides composed of a mixture of $NiFe_2O_4$, Fe_3O_4 and $FeCr_2O_4$. Consequently in the high temperature RCS, the internal surfaces of the low alloy steel pressure vessel, pressurizer and steam generator are clad with type 308/309 stainless steels. However there are carbon steel components exposed to high temperature water/wet steam such as feedwater piping, main steam lines and some parts of the pressure vessel left exposed following repair procedures at, for instance, penetrations.

Because of the dependencies of corrosion rate and oxide solubility on pH, the water chemistry specifications for PWR's impose a tight control on the pH values, which may vary slightly from one plant to another, and between primary [see Appendix B.11] and secondary [see Appendix B.12] systems. This control is achieved via injection from the Chemical Volume and Control System (CVCS) to the primary system of LiOH, and boric acid (for chemical shim control of

core reactivity). Early water chemistry specifications imposed a pH_{300C} specification of 6.9 +/- 0.2, corresponding to the minimum in magnetite solubility (Figure A.7), but more recent specifications have increased this pH_{300C} specification range to 7.1-7.3, in order to take advantage of both the corrosion resistance due to nickel ferrite and the improved control of crud build up and shutdown dose rates. There is a limit to which this alkalinity increase can be allowed which is associated with an increase both in corrosion rate of zirconium alloy fuel cladding, and in susceptibility to stress corrosion cracking of Alloy 600 steam generator tubing.

In addition to pH control for PWRs associated with the thermodynamic stability of a protective oxide on the surface, the kinetics of corrosion are also, as discussed in section A.3, a function of the presence of oxidizing species. Consequently, the RCS primary system has a considerable overpressure of hydrogen to minimize the reduction kinetics of Equation A.7. A maximum limit in the amount of hydrogen overpressure is determined by avoidance of hydriding of the zirconium alloy cladding. This overpressure also ensures that, under normal operating conditions, boiling in the reactor core is suppressed, thereby minimizing the possibility of concentration of, for instance, impurities at heat transfer surfaces in the primary side and the consequent increase in corrosion rate at these boiling sites.

In the secondary system the dissolved oxygen concentration (which affects both the activation and diffusion controlled reduction kinetics and, thereby, the metal corrosion rate), is controlled by the presence of hydrazine [see Appendix B.12]. However since boiling occurs on the secondary side of the steam generator tubes, it is possible to have accelerated corrosion in occluded regions such as tube/tube support regions; this will be discussed later in the section on crevice corrosion.

Control of general corrosion in the lower temperature systems such as the service water system, where the piping is predominately carbon steel, can present a potential problem since the water supply for such systems are “uncontrolled” sources such as the ultimate heat sink, lake water or sea water. Moreover, under such lower temperature conditions the surface oxide is not as protective as that at higher temperatures in the pH range specified for, for instance, the RCS. However generally accepted corrosion prevention methods, widely used in other industries (transportation, petrochemical, marine, etc.) are applied, including the use of cathodic protection, (for, e.g. submerged pumps and underground piping), inhibitors (such as phosphates) or biocides to control microbiologically induced corrosion.

Chemistry control for general corrosion in direct cycle BWRs is largely driven by the fact that, under “normal water chemistry” (NWC) conditions, there is an excess of dissolved oxygen in the coolant, since the other product of the radiolytic breakdown of water, hydrogen, is preferentially partitioned to the steam phase. This dissolved oxygen has a deleterious effect on stress corrosion cracking of most of the BWR materials of construction, as discussed later. Consequently the main driving force in chemistry control for BWRs [see Appendix B.10] has been to lower the dissolved oxygen concentration (or more accurately, the corrosion potential) by both injection of hydrogen (**H**ydrogen **W**ater **C**hemistry) and control of the dissolved impurity level. As a result of this industry action, the level of impurity contents in the reactor coolant has dropped markedly over the last few decades, with current coolant conductivities approaching that of theoretically pure water (Figure A.8); moreover, virtually all of the US BWRs now operate under HWC with

modifications due to the addition of noble metals (Noblechem™) to the coolant that improve the efficiency of the oxygen/hydrogen recombination [see Appendix B.10, 10, 11].

Although these actions have been extremely effective in controlling stress corrosion, the addition of hydrogen does have an impact on radioactivity release due to ^{16}N during power operation and the creation and release of activated corrosion byproducts, mainly ^{60}Co, during plant shutdown or changes in between NWC and HWC. In the former case the release of ^{16}N to the steam and off-gas systems is aggravated by the addition of hydrogen to the coolant and the effect that this has on the formation of volatile nitrogen bearing species originating from $^{16}O(n,p)^{16}N$ reactions in the core region. This increase in the ^{16}N content effectively limits the hydrogen addition to the feedwater to 200-300 ppb. In more recent times the widespread adoption of noble metal technology, and especially Noblechem™, has minimized the HWC/^{16}N problem and has allowed the efficient suppression of the corrosion potential without the deleterious radioactivity offgas release.

The creation and release of ^{60}Co is directly relatable to the presence of ^{59}Co in corrosion products from cobalt-rich, wear resistant Stellite valve seatings, roller bearings, etc, or to cobalt impurities in the stainless steel piping and, especially, control rod blade sheaving. Once this crud is deposited and the ^{59}Co is activated on the fuel cladding, the resultant ^{60}Co is transported to the stainless steel piping where it is incorporated into the oxide spinel structure. The mitigation for this deleterious general corrosion related phenomenon is to (a) reduce the cobalt inventory in the reactor circuit by using alternatives to cobalt-rich Stellites, (b) minimizing the crud formation (which acts as a transport vehicle for the activated ^{60}Co from the core to the piping) by control of the anionic impurity and the dissolved iron concentrations and, (c) making zinc additions, of the order of 10-100ppb, to the coolant. In this latter case the zinc inhibits the corrosion of stainless steel, resulting in thinner spinel films, and also takes up competing sites where ^{60}Co could reside in the oxide spinel structure.

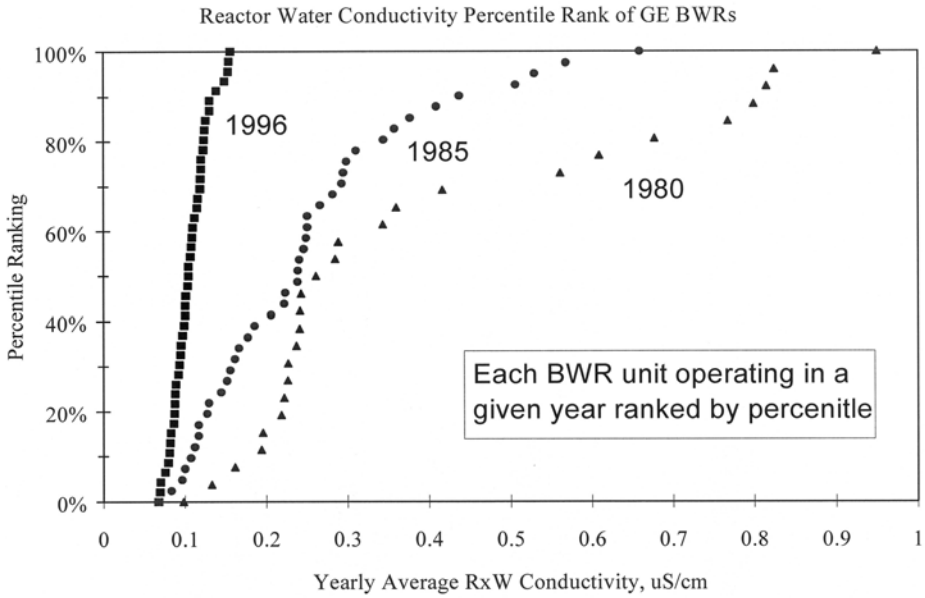

Figure A.8 Change in reactor coolant conductivity in BWRs [ ]

Although the reduction in dissolved oxygen content and corrosion content via HWC/ Noblechem™ has been successful in reducing the extent of stress corrosion cracking in BWRs, it has introduced a problem of increased corrosion of carbon steel feedwater lines [12,13] due to the formation of non-protective magnetite films at the low corrosion potentials associated with oxygen contents <5-10 ppb. Consequently BWR water chemistry guidelines [see Appendix B.10] specify a minimum dissolved oxygen content of 30 ppb in the feedwater lines to ensure the creation of a more adherent and protective magnetite film which is stable at the more elevated corrosion potentials.

From a life-management standpoint it is apparent that the knowledge base exists to predict and control the general corrosion behavior in most of the materials of construction in LWRs. Indeed there is some considerable margin in the design basis to account for general corrosion since actual corrosion rates are significantly below the design-basis allowable values. For instance, the design specification provides a general corrosion allowance of 120 mils for the carbon steel main steam system. The actual general corrosion rate for carbon steel piping in a steam environment is less than 0.16 mils per year. Similarly, the corrosion allowance for stainless steel piping operating in the 500-600°F range is 2.4 mils. The actual general corrosion rate for stainless steel in this temperature range is 0.01mils/year of service life.

Boric Acid Corrosion

Although, as discussed in the section above, the general corrosion rates of the LWR materials of construction are well below the design values required to maintain structural integrity, and the radioactivity issues associated with activation of the corrosion products can be managed, there are situations where very high corrosion rates can occur over significant areas.

One such situation is the corrosion of carbon and low alloy steels due to boric acid in PWR primary environments [see Appendix B.18, 14, 15]. Under normal operating conditions the corrosion rate of carbon and low alloy steels in borated, hydrogenated, primary water is <0.025 mm/year, but problems have occurred in operating plant when borated water leaks from the PWR RCS onto an external carbon or low alloy steel surface. Under these leakage situations the boric acid concentration on the external component will increase due, for instance, to steam flashing and alternate wetting and drying cycles that produce, ultimately, a low pH boric acid slurry which, in combination with an air atmosphere, can cause very high corrosion rates of approximately 25mm/year,(Figure A.9). Such an increase in corrosion susceptibility is predictable via reference to the Pourbaix diagram for the iron/water system (Figure A.1), which indicates that, under acidic, and especially under higher surface potential, oxygenated conditions, corrosion is likely, and that it is unlikely that any protection due to a surface oxide would be forthcoming given the high oxide solubility under these conditions (Figure A.7).

Problems of boric acid wastage of closure studs in the pressurizer, reactor coolant pump, steam generator manways, etc. have been associated with leaks due to gasket failures, with the most notable recent observation in 2002 being the through-wall corrosion of the pressure vessel head at Davis Besse associated with stress corrosion cracking of nickel-base alloys in the vessel head penetration assembly and subsequent leakage of primary coolant into a restricted geometry

configuration with the result that boric acid concentrated to levels that lead to excessive corrosion of the low alloys steel pressure vessel.. All of these incidents are in the higher temperature RCS. By contrast, boric acid wastage problems would not be expected to be associated with leaks in lower temperature systems (<212°F) such as the ECCS and CVCS since, although these systems are borated, there would be no mechanism to concentrate the boric acid sufficiently to achieve the low pH values needed for high low alloy steel corrosion rates.

As indicated in Figure A.9 the corrosion rate of carbon and low alloy steels increases with increasing acidity and may, depending on the pH value be greatest at temperatures between 80 and 150°C. Such a surface temperature range is achievable due to evaporative cooling of the escaping high pressure coolant impacting on the external component.

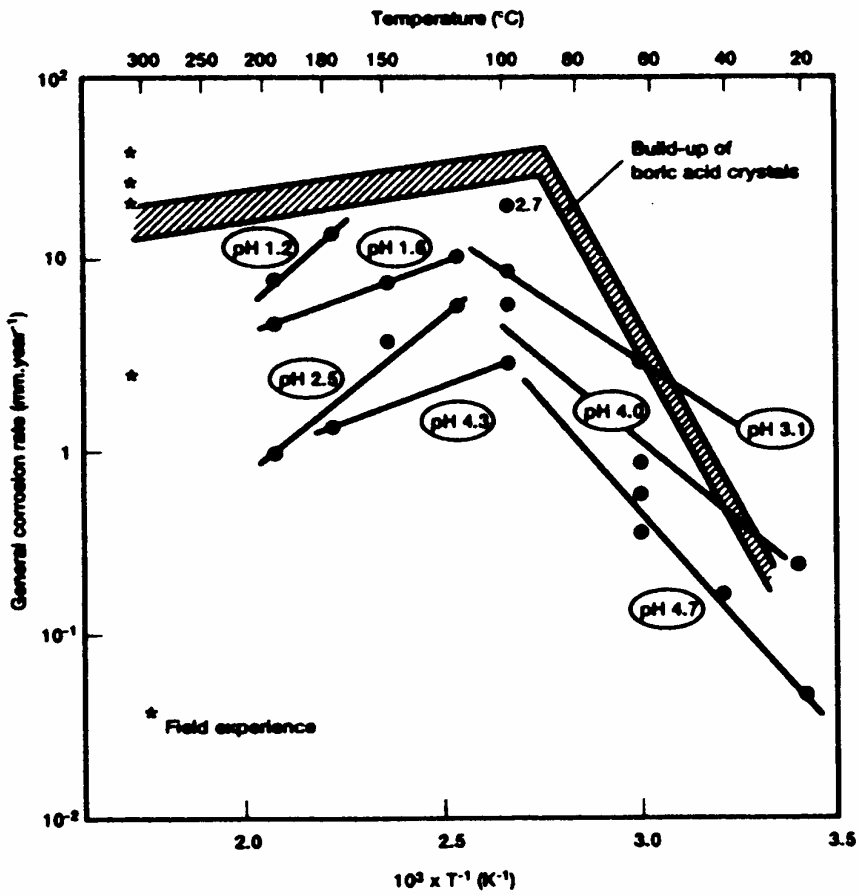

Figure A.9. Relationship between the corrosion rate of carbon and low alloy steels in various acidified boric acid solutions as a function of temperature. [20]

As discussed in Appendix B.18, the Davis Besse incident does present some challenges to the assertion that all boric acid wastage is predictable. As a result there are ongoing research efforts both in the industry and the NRC to determine, for instance, the interactions between the

corrosion rate and various factors such as the leakage rate (and the role of erosion –corrosion or impingement), chemistry of the escaping coolant, extent of evaporative cooling of the low alloy steel surface, and the role of the geometry of the assembly (the annulus between the CRDM tube and the pressure vessel in the case of Davis Besse), which will affect the mass transport of oxygen and liquid within the crevice.

Flow-Accelerated Corrosion and Erosion-Corrosion.

Flow-accelerated corrosion is frequently localized at areas of high turbulence, often associated with geometrical discontinuities or abrupt changes in flow direction, and this manifests itself as a localized wall loss. There are well-defined electrochemical and mechanical reasons for such degradation since the water or steam flow past the metal component may increase the kinetics of corrosion in various ways.

At the simplest level the corrosion kinetics may be increased under both laminar and turbulent flow regimes due to an increase in diffusion rates of, for instance, dissolved oxygen, to the metal surface, or the increase in removal rate of oxidized species from the metal surface. These concepts were discussed in relation to Figure A.4. If the oxide film has a two layer structure, as seen and discussed above for the general corrosion of carbon and low alloy steels in high temperature water, (Figure A.10), then increasing flow rate may also remove the outer oxide layer under turbulent flow conditions. Under these conditions the flow-accelerated corrosion rates will be controlled ultimately by the reductive dissolution of the inner oxide layer and the diffusion kinetics of Fe(II) species away from the surface. Under such conditions the corrosion rate may be considerably enhanced and be of the order of 10 mm/year.

It is apparent that these controlling conditions are electrochemical in nature. It is also possible to accelerate the corrosion rate even further by imposing a mechanical factor to the removal of the outer oxide layer, including the effect of the impact of water droplets on the surface in two phase flow steam systems (e.g., wet steam in main steam lines or cross around piping in turbines), cavitation effects (e.g., impeller blades in pumps) or, in extreme situations, entrained particles, such as sand, in service water systems. Such mechanically dominated effects are normally described as “erosion-corrosion” or “erosion” depending on the degree of the mechanical contribution.

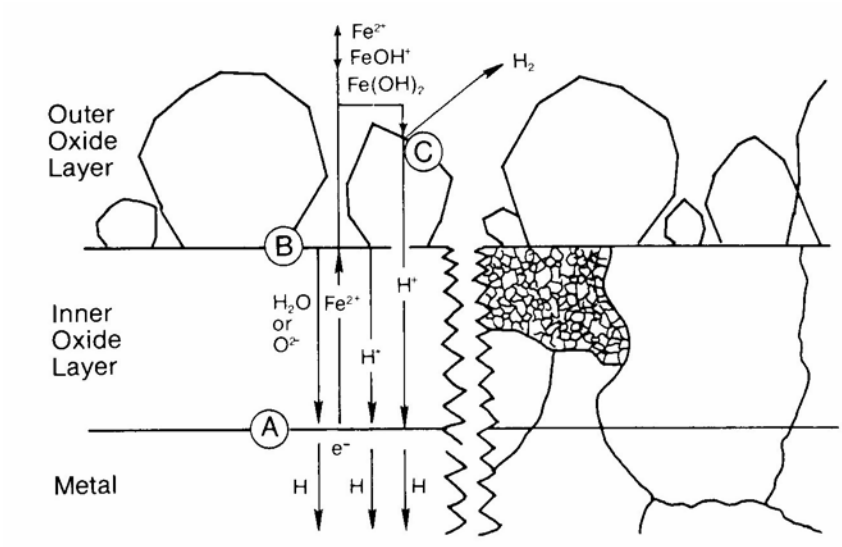

Figure A.10. Schematic of two-layer oxide structure on carbon steel in high temperature water. [16]

As mentioned above the extent of flow-accelerated electrochemically-controlled corrosion in high temperature aqueous environments is very much a function of the material/environment combinations that affect the structure of the oxide layers and their chemical and mechanical stability. Following the catastrophic failure of a carbon steel suction line to the main feedwater pump at Surry-2 PWR [17], there was considerable study [18] of the factors controlling flow accelerated corrosion in LWRs, leading up to the development by EPRI of the CHECWORKS™ prediction code [19]. As discussed in more detail in Appendix B.17, the flow rate effect on the corrosion rate for carbon or low alloy steels is a function of the material composition, piping geometry, single vs. two-phase environment, temperature, pH, laminar vs. turbulent flow and the local corrosion potential. As indicated in Figure A.11 for flow accelerated corrosion in deoxygenated ammoniated water, the corrosion rate is a non-monotonic function of temperature, with a maximum occurring in the range of 130-150°C for single phase fluids; the peak corrosion rates occur at a higher temperature range for two-phase environments (e.g. wet steam in the main steam line and turbine cross around piping).

Control of the local corrosion potential (or dissolved oxygen content) is a key factor in managing flow accelerated corrosion of carbon and low alloys steels in the main steam, feedwater, condensate and moisture separator piping in BWRs. As indicated in Figure A.12, the flow-accelerated corrosion rates in condensate and moisture separator reheater drain systems are a function of the local dissolved oxygen content; such an observed relationship is in agreement with the CHECWORKS™ predictions.

The ability to minimize the corrosion rate by maintaining the local dissolved oxygen content above 30 ppb will be a function of the amount of air in-leakage from the turbine condenser and, as mentioned earlier in the general corrosion section, the degree of oxygen dosing in the feedwater lines. The amount of oxygen control required minimizing flow-accelerated corrosion

in the two-phase wet steam main steam line will be a function of the amount of radiolysis occurring in the reactor core, the degree of hydrogen water chemistry/ Noblechem™ and the extent of venting being applied in the moisture separators. The ultimate remedy is to make use of the more protective and adherent films associated with chromium alloying; hence the replacement of the susceptible lines with low alloy steels with higher chromium content, stainless steels or to use a higher chromium content coating deposited by thermal spray or weld overlay.

The message here is that the extent of flow-accelerated corrosion that can occur in carbon and low alloy steels in PWRs and BWRs is predictable and the mechanism is understood. The prediction algorithms (i.e.CHECWORKS™) are routinely used in individual plant Aging Management Programs to assign inspection priorities. It has generally been found that, where problems do occur, it is apparent that these analysis and inspection priority methodologies have not been followed.

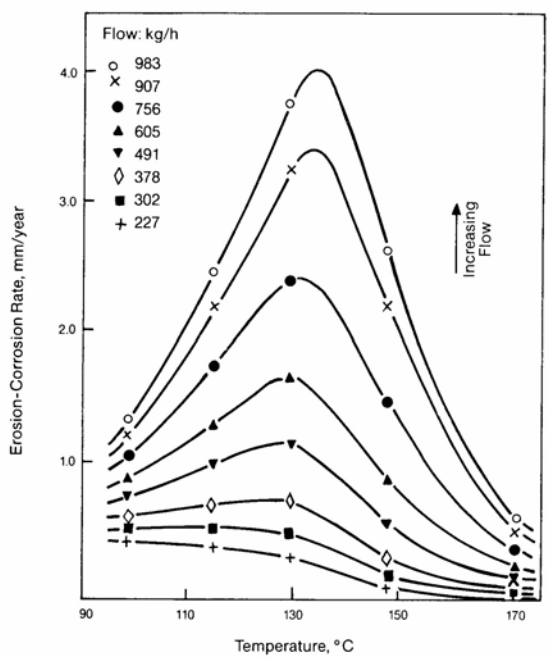

Figure A.11. Effect of temperature on the flow accelerated corrosion rate of carbon steel in deoxygenated ammoniated water. [20]

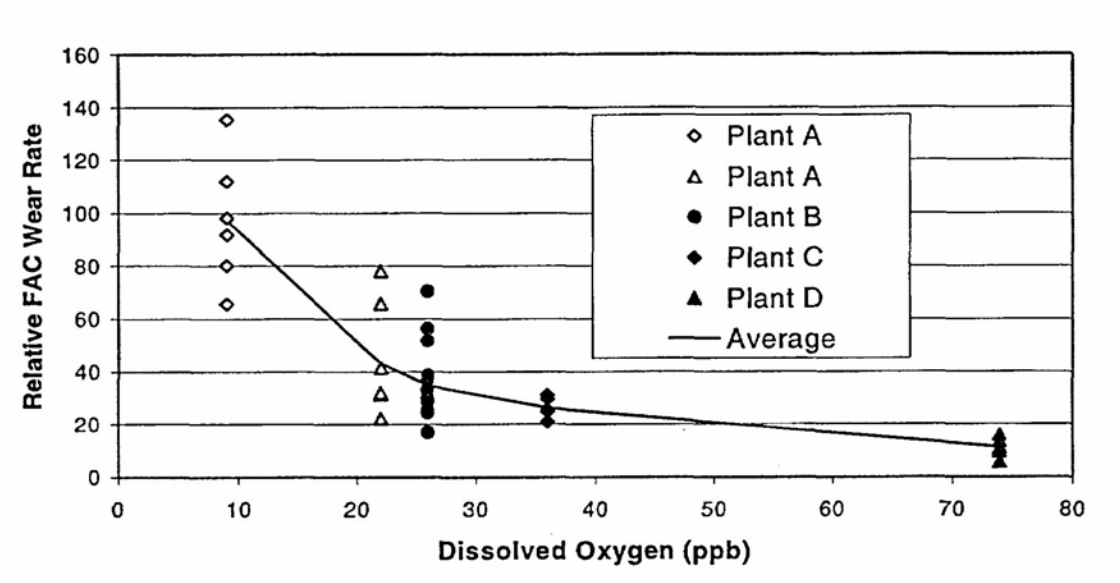

Figure A.12. Flow-accelerated corrosion data for condensate and moisturizer separator reheater drain systems in four BWR plants as a function of the local dissolved oxygen contents [Appendix B.10]

A.4.2 Localized Corrosion

This section addresses materials degradation modes, where the degradation occurs over relatively small areas but, potentially, may occur at high penetration rates. The result in such cases may be localized leakage or, in more extreme situations, lack of structural integrity and catastrophic failure. Such degradation modes include, crevice, pitting, galvanic and microbiologically induced corrosion and environmentally assisted cracking. This latter category includes stress corrosion cracking, strain-induced cracking and corrosion fatigue (which is discussed in the section on Fatigue).

Crevice Corrosion

As the title suggests, this phenomenon is associated with crevices in which a stagnant solution is present and where there is a mechanism to make that solution more aggressive vis a vis the metal corrosion rate (e.g. increased acidity and increased anionic impurity concentration). The crevices may be inherent in the component design (such as at gaskets, lap joints, bolt heads and threads), or may occur under corrosion deposits and sludge piles. The critical factors in controlling this form of attack are; (a) the geometry of the crevice, and the conditions that affect the thermal hydraulics within the crevice such as the flow direction and rate past the mouth of the crevice and; (b) the mechanisms that affect the cationic and anionic concentrations within the crevice.

The thermal hydraulics and mechanisms of crevice corrosion have been extensively researched over the last 30 years and, as a result, control techniques are available (see, for instance, References 21 and 22). Examples of this understanding/control synergy are given below.

As indicated schematically in Figure A.13 there is the possibility that, in aerated solutions, the site for oxygen reduction is concentrated at the exposed surface at the mouth of the crevice. A reason for this is that the convection-controlled transport rate of dissolved oxygen into the crevice is insufficient to make up for the removal of dissolved oxygen due to general corrosion on the crevice sides. The resultant separation of the oxygen reduction site at the crevice mouth from the metal oxidation site at the tip of the crevice imposes a potential gradient down the crack, thereby giving rise to potential-driven diffusion of anionic impurities (e.g.chloride) to the crevice tip. In order to maintain electroneutrality it is necessary that there be an increase in acidity within the crevice due to, for instance, the hydrolysis of the dissolved metal cations (Equation A.4) and, thus, the environmental conditions (low pH, high anionic impurity concentration) are created at the crack tip for an increase in metal corrosion rate.

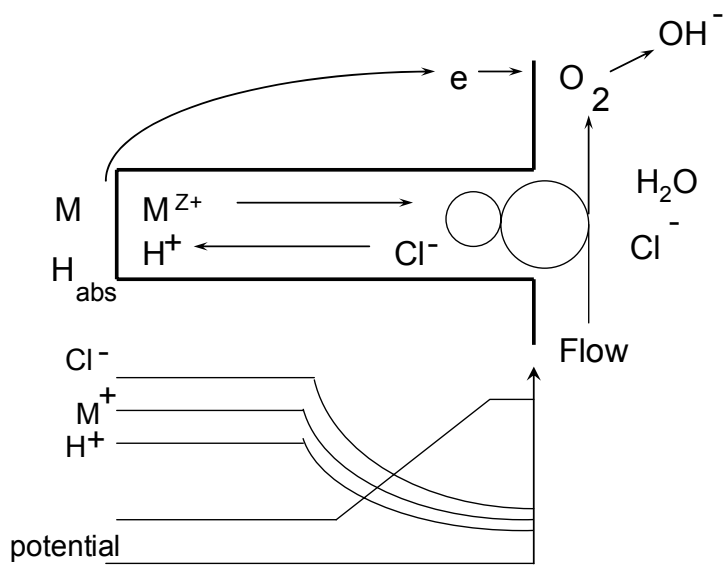

Figure A.13. Schematic of crevice in aerated solution, indicating the separation of the metal oxidation and oxygen reduction sites, and the consequent changes in pH and anionic concentrations [ ]

A further crevice corrosion mechanism is possible at heat transfer surfaces, where concentrations of species may occur due to their distribution between the aqueous and gaseous (e.g. steam) phases or the evaporation of volatile species. This concentration of acidity, alkalinity or other aggressive ions (depending on the specific system) may be retained under specific geometrical conditions which inhibit solution redistribution. A classical example of this is the localized corrosion of carbon steel tube support plates in PWR steam generators, as illustrated in Figure A.14 [see Appendix B.7], which has led to denting of the Alloy 600 tube and subsequent stress corrosion cracking on the primary side of the tube.

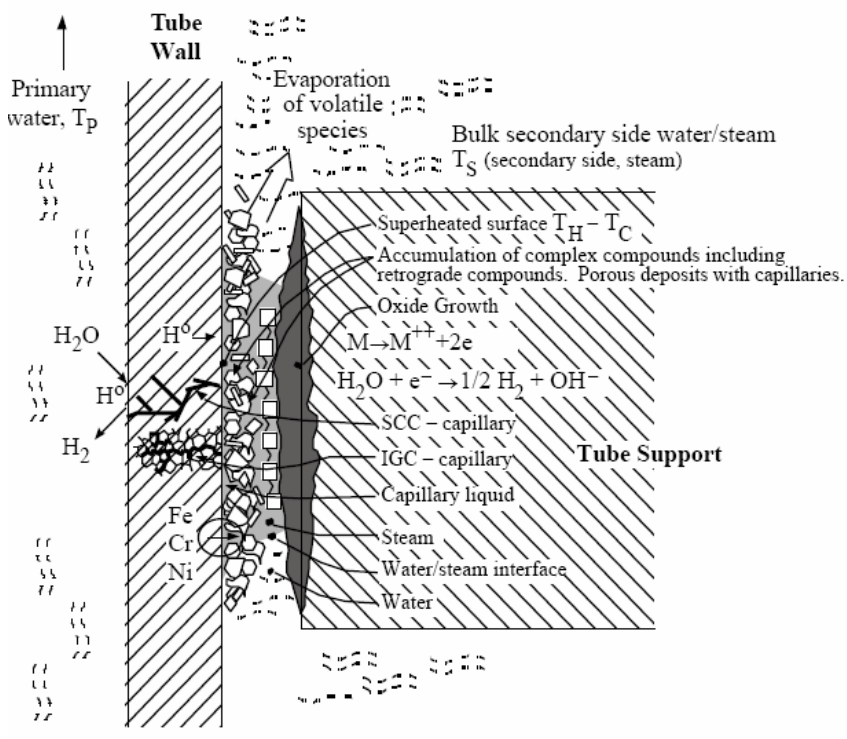

Figure A.14. Schematic of crevice formed at PWR steam generator tube/ carbon steel tube-support, together with the phenomena that give rise to the localized corrosion. [23]

Such understanding of the mechanisms of crevice corrosion lead to logical methods of controlling the problem including, for instance, ensuring that there is adequate flow in the crevice, as illustrated by the redesign of BWR pressure vessel inlet safe ends and steam generator tube support structures, and by the control of the amount of oxidant in the environment at the mouth of the crevice. Examples of this latter control method are the adoption of hydrogen water chemistry/ NobleChem^{TM} in BWRs, and the appropriate use of hydrazine in PWR secondary systems. The hydrogen overpressure in a PWR reactor coolant system provides adequate protection against crevice corrosion for the internal surfaces of RCS components. As indicated in Table A.5, residual concerns for control of crevice corrosion are mainly for carbon steels, which have an inherently weaker corrosion resistance (compared with austenitic alloys) in the aggressive environments in the crevices and, especially, in systems where it may be more difficult to control the creation of the water chemistry in the crevice, such as in aerated service water systems or at restricted heat transfer sites in the secondary side of steam generators. It should be pointed out, however, that other forms of localized degradation such as stress corrosion cracking or intergranular attack in stainless steels and nickel-base alloys can be accelerated in crevice environments.

Pitting Corrosion

Pitting corrosion has very similar attributes to crevice corrosion in that it depends in part on the creation of a localized environment; however the important difference is that the geometric features that lead to degradation are inherent in the material microstructure and may be manifested by long incubation periods before the pits grow. Again this is a topic that has received much attention and research [8, 21, 22, 24, 25] over many decades and is covered in part in a topical report [see Appendix B.3]. Thus the overall judgment in Table A5 is that there is adequate understanding to manage this phenomenon in LWRs, with the biggest uncertainty being associated with systems where there might be lesser knowledge or control over the environmental conditions.

Quantitative models for predicting and controlling pitting corrosion in nuclear systems focus on taking into account the following sequence of events:

(a) Localized breakdown of the surface oxide, usually due to the presence of aggressive anions. The aggressive anions are normally associated with chlorides originating from, for example, condenser leaks, but damage can also be associated with other halides, sulphates, perchlorates, etc.. The metallurgical sites for such oxide breakdown may be random, but are usually associated with inhomogeneities such as surface breaking precipitates or with grain boundaries over which the oxide is of a less protective nature. The breakdown of the oxide occurs at surface potentials above a critical value (known as the "pitting potential"), which is a function of the anion type and its concentration, the material composition, temperature, etc. Thus pitting is of a potential concern if the corrosion potential is more positive than the pitting potential, and such a criterion puts a limitation on the system conditions under which pitting corrosion would be a problem This is illustrated in Figure A.15 by the temperature dependence of the corrosion potential and pitting potential of Alloy 600 in water containing various concentrations of chloride. It is seen that under low dissolved oxygen conditions the corrosion potential is always lower than the pitting potential (for the indicated range of chloride concentrations) and, therefore, over a wide temperature range, pitting should not be a concern. At higher oxygen content conditions, however, pitting might be a concern, especially at lower temperatures and at higher chloride concentrations.

The pitting potential will also be a function of alloying content (and therefore the extent of passivity or corrosion resistance) and will increase with both chromium content and molybdenum content; thus nickel-base alloys and ferritic or austenitic stainless steels (and especially molybdenum-containing type 316 stainless steel) will exhibit better pitting resistance than lower alloyed materials.

(b) Once the conditions for oxide breakdown have been met, then localized corrosion, or pit growth, may occur at a rate that is, amongst other parameters, a function of the degree that the potential exceeds the pitting potential, and the maintenance of the aggressive environment in the growing pit (i.e. the conditions discussed in the section on crevice chemistry).

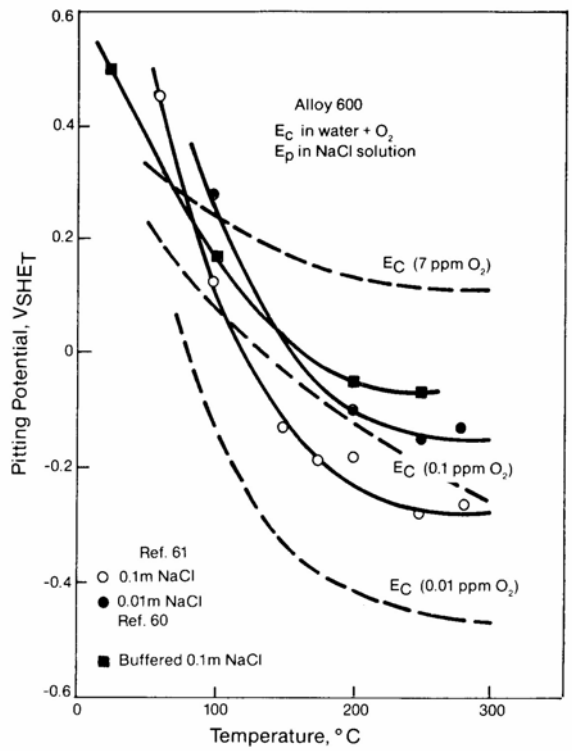

Figure A.15. Pitting and corrosion potential for Alloy 600 in water containing chloride anions as a function of temperature. [26, 27]

Although the essential controlling parameters of importance in the initiation and growth of pits are known, it is also apparent that many of these parameters are dependent on random events [28, 29] and that, therefore, there will be a distribution associated with both the stochastic [28, 29] and deterministic model [30, 31] predictions. Such effects on the variability in predictions are discussed in separate topical reports [see Appendices B.15 and B.19]. Regardless of these aleatory uncertainties, the basic knowledge of the conjoint conditions for pit initiation and growth exists in order to manage potential pitting damage in LWR systems. This knowledge includes the material choice and degree of environment (water purity, flow rate) control that is needed. Prediction uncertainties arise when there are unanalyzed changes in plant configuration; an example of this might be the removal of certain insulation materials from stainless and carbon steel piping, for, for instance, mitigation of sump pump blockage concerns, when the chemical makeup of that insulation material might be conferring pitting (and stress corrosion cracking) resistance to the piping.

Galvanic Corrosion

Galvanic corrosion is the loss of material, generally measured as a ***local*** rate of loss of surface material, caused when two materials with substantially different electrochemical corrosion potentials are in electrical contact in the presence of a corrosive (and electrically conductive) environment. In such cases the corrosion rate of the more active material (i.e., that with the more negative corrosion potential) is increased, with the magnitude of that increase being a function of

the relative areas of the two metals, and the difference in corrosion potentials. Thus the corrosion rate of mild steel condenser tube sheets exposed to seawater will be increased in the area adjacent to a copper based condenser tube that is rolled into it by a factor of X3-7 depending on the excess area of the copper tubes. Similarly carbon and low alloy steels have substantially lower electrochemical potentials relative to stainless steels and titanium alloys, and would be preferentially attacked in a galvanic couple.

As with general corrosion, galvanic corrosion is a well-understood phenomenon, being the theoretical basis for sacrificial anode protection techniques used in many industries. Consequently, although the possibility of galvanic corrosion exists, it is relatively rare in reactor service since the corrosion potentials of the various materials in the higher temperature systems are reasonably similar, and in the lower temperature systems involving large surface areas in cooling water such as condensers [32] the phenomenon is generally accounted for at the reactor design and construction stage.

Microbiologically Influenced Corrosion (MIC)

MIC is associated with the presence and biological activity of various bacteria and fungi which, upon interaction with nutrients in the environment, produce organic acids which may lower the local pH level to 2.5 thereby increasing the metal corrosion rate (Figure A.1). The "environment" in this case may be not only untreated service water, for example, but also greases applied to external structures for general corrosion protection [33]. Damaging species other than organic acids may be formed which are specific to the bacteria and fungi microorganism [see Appendix B.16]. For instance, anaerobic sulphate-reducing bacteria (SRB) produce reduced sulphur compounds that may increase the localized corrosion rate of carbon and low alloy steels, and aerobic bacteria, which require oxygen for survival, are sulphate oxidizing, producing sulphuric acid, and a local increase in acidity. In addition such bacteria form slimes, which cover the metal surface, thereby creating an oxygen-starved region for the development of anaerobic bacteria. In such cases, biological fouling can be so severe that it not only forms corrosive crevices, but can also block flow in service water piping.

These various bacteria each have very specific conditions of survival in terms of pH, temperature, dissolved oxygen content and supply of appropriate nutrients. From a control viewpoint, however, MIC is not expected for any extended period at temperatures above 99°C or in borated- or hydrazine treated water. For instance, treated water systems, such as PWR borated emergency core cooling systems, have operated for many years with no evidence of MIC. However, damage might be expected in cooling water and service water systems that have a flow rate low enough to ensure an adequate nutrient supply rate without physically removing the bacteria. Another process that exacerbates MIC is the intermittent flushing of water lines that are otherwise stagnant, such as fire protection lines. The periodic flushing introduces new nutrients to the stagnant lines, increasing biological activity and increasing the risk of bacteriologically induced corrosion and fouling. Consequently, MIC damage has been observed in LWR structures such as carbon and stainless steel piping and tanks, copper-nickel, stainless steel, brass and aluminum bronze cooling water pipes and tubes, especially during construction and, hydrotest and outage periods [4]. Effective control in these potentially susceptible systems is achieved by the use of biocides and controlling the nutrient supply rate.

Environmentally Assisted Cracking

Environmentally assisted cracking is closely related to the principles of other localized corrosion phenomena, such as pitting, crevice corrosion and intergranular attack, and these may well act as the precursor [see Appendix B.15] to sustained crack initiation and growth when that localized corrosion process has the added contribution of tensile stress.

Environmentally assisted cracking phenomena cover a wide spectrum of degradation modes, categorized in terms of stress corrosion cracking, hydrogen embrittlement, strain-induced cracking and corrosion fatigue. Even within these categorizations there are submodes that may be defined in terms of the morphology of cracking (transgranular, intergranular, interdendrittic, granulated), the effect of specific environments (irradiation, "external, contaminated", primary-water) or subsets of an existing cracking mechanism (low-temperature crack propagation as a subset of hydrogen embrittlement). To a large extent such a confusing categorization has arisen because of the historical nature of the first laboratory and reactor observations, plus the fact that, at that time, it was not recognized that many of the cracking modes were not new mechanisms, per se, but merely associated with changes in a rate controlling parameter. For instance, as shown in Figure A.16, the subcritical crack propagation rates in stainless steels strained at various rates in oxygenated water at 288°C have a monotonic relationship with strain rate; those observed at slow strain rates, associated with creep under constant load (e.g. stress corrosion cracking), are an extension of both those observed under applied, monotonically-increasing strains (e.g., strain induced cracking), and those at even higher applied strain rates under cyclic loading (e.g., corrosion fatigue). Thus, for this system, there is no difference in the crack propagation mechanism for these cracking modes, although the sensitivity of the cracking response to e.g. environmental or material conditions may change significantly. Similarly the effects of irradiation on the cracking susceptibility are now recognized as merely changing the rates of various rate-controlling parameters, rather than introducing an entirely new mechanism of crack propagation.

It has long been recognized that there are three conjoint requirements for environmentally assisted cracking to occur; a "susceptible" material condition, an "aggressive" environment and a tensile stress. The extent of the conjoint requirement will change with the specifics of the system but, in general, if one of these attributes is absent then the cracking phenomenon will not occur; this very qualitative observation was the root of many of the early mitigation actions for, for instance, stress corrosion.

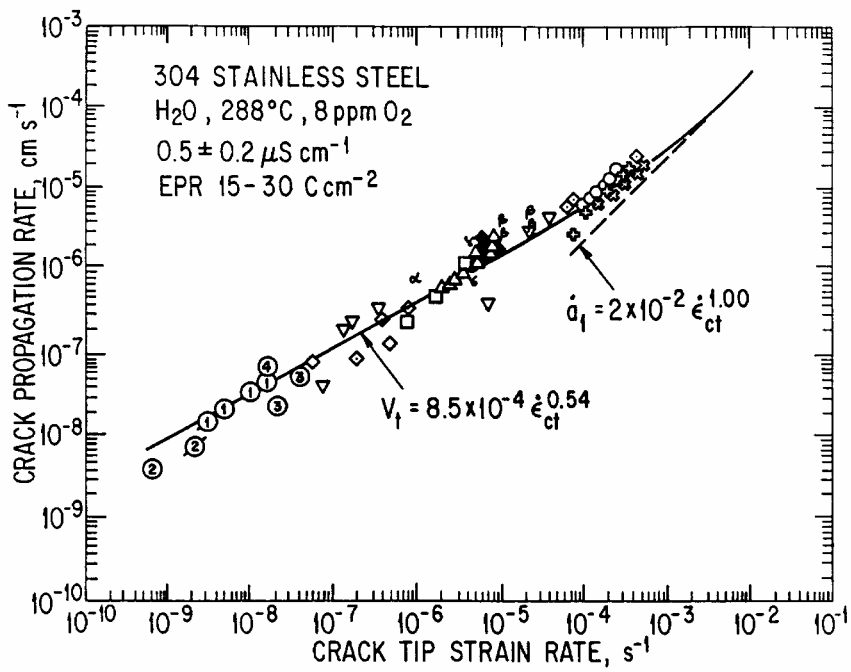

Figure A.16. Observed and theoretical crack propagation rate vs. crack tip strain rate relationships for sensitized 304 stainless steel in oxygenated water at 288°C. Note that the numbered data at the lowest crack tip strain rates were obtained under constant load or displacement conditions, whereas the data marked by geometric symbols were obtained under cyclic loading. Intermediate data, identified by Greek symbols where obtained under monotonically rising "slow strain rate" conditions [34, 35]

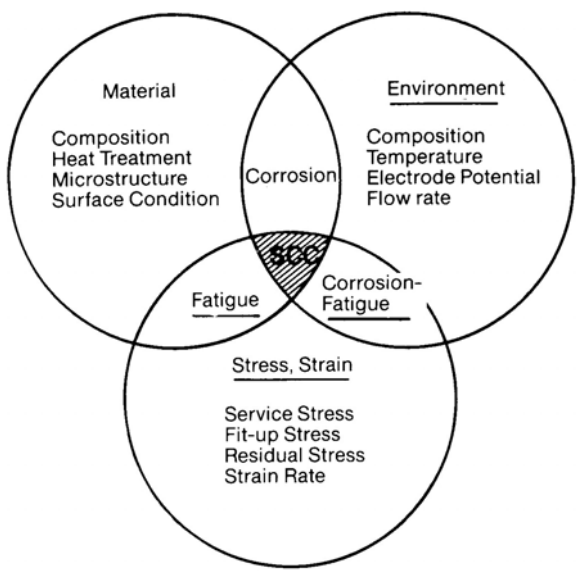

Figure A.17 Conjoint material, stress and environment requirements for stress corrosion cracking [36]. An expanded list of some of the contributing factors was given in Figure 4.4

The management of environmentally assisted cracking has moved in the last 25 years beyond reliance on a largely qualitative understanding of the various phenomena inherent in Figure A.17, to the development of a quantitative understanding of the multidimensional interactions between the parameters that control the cracking susceptibility, backed up by an understanding of the mechanisms of crack initiation and propagation. Such developments are central to the definition of appropriate inspection procedures required by current regulations. The fact that the system parameters are not always well enough defined, and the interactions between these parameters are not always well quantified or understood from a mechanistic viewpoint, is the basic reason why stress corrosion cracking appears as a potential concern area for so many of the reactor systems in Table A.5.

The challenges in predicting the occurrence of environmentally assisted cracking were discussed in Sections 2.5 and 4.2, and several topical reports listed below address specific issues associated with, for instance, irradiation, the overall environment and the alloy composition:

- SCC of Sensitized and Non-Sensitized Austenitic Stainless Steels and Weldments [see Appendix B.1]
- IASCC of Stainless Steels and Other Irradiation Phenomena [see Appendix B.2]
- SCC of Alloys 600, 690, 182, 152 and 52 in PWR Primary Water [see Appendix B.6]
- Corrosion of Steam Generator Tubes [see Appendix B.7]
- Stress Corrosion Cracking of Carbon and Low Alloy Steels [see Appendix B.8]
- Environmental Degradation of High Strength Materials [see Appendix B.9]
- Degradation of Fracture Resistance; Low Temperature Propagation (LTCP) in Nickel-Base Alloys [see Appendix B.13]

In many of these systems there is a considerable database to allow analysis of the effects of system variables on the cracking response. In some cases, however, there is cause for concern about the data quality (due to lack of experimental control during older data collection), which gives rise to excessive data variability and, therefore, uncertainty in the predictions of future behavior. In other cases the variability is to be expected due to the stochastic nature of some of the cracking phenomena [see Appendix B.7] and, in such cases, there are well-accepted data analysis techniques [see Appendix B.19] to address this. In other systems (such as stress corrosion cracking of carbon and low alloy steels [see Appendix B.8] and austenitic stainless steels under unirradiated [see Appendix B.1] and irradiated [see Appendix B.2] conditions), there is sufficient mechanistic understanding of the effects of the various system variables to give assurance that the cracking behavior in the future may be adequately managed. However, in other systems (such as stress corrosion cracking of some nickel base alloys in PWR primary coolant [see Appendix B.6] at operating temperatures, or under dynamic straining conditions at lower temperatures [see Appendix B.13], there is a need for further development of mechanistic understanding of the cracking process.

The following discussion presents a relatively high level treatment of some of these topics in order to provide a skeleton for the details given in these topical reports. Focus is placed on certain aspects of environmentally assisted cracking which are highlighted in the PIRT panel judgments; namely changes in the morphology of cracking (transgranular vs. intergranular), the

effect of environment (effects of irradiation and PWR primary water) and "new" modes of cracking (low temperature crack propagation).

Intergranular Stress Corrosion Cracking (IGSCC)

IGSCC is associated particularly with the cracking of austenitic stainless steels and has been widely experienced in high-purity water in BWR piping (Figure A.18) and internals. Under these conditions the conjoint requirements for cracking given in Figure A.17 correspond to an environment that is oxidizing (due to an excess of radiolytically-produced oxygen or hydrogen peroxide), a microstructure that is "sensitized" (due to thermal sensitization during welding and/or stress relief heat treatment) to produce a chromium depleted region adjacent to the grain boundary, and a tensile stress associated primarily with weld residual stresses.

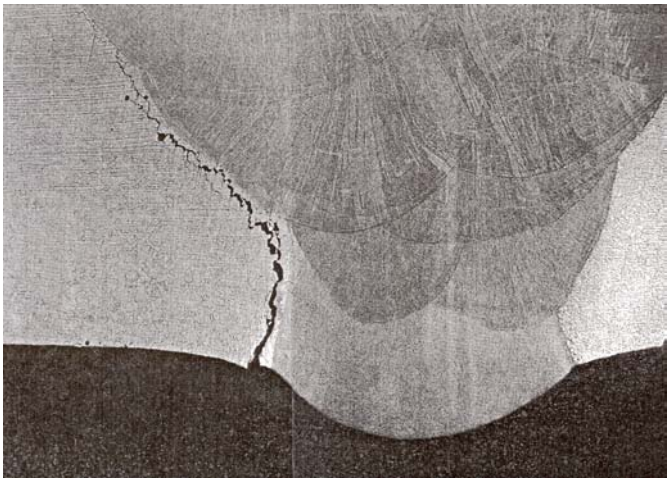

Figure A.18. IGSCC in a 400mm.(16 ins.) diameter welded Type 304 pipe exposed to oxygenated water at 288°C. Note propagation adjacent to the weld heat affected zone, in a region associated with maximum grain boundary chromium depletion and weld residual tensile stress [37 ?]

IGSCC has been extensively researched [36] and is considered, at least for austenitic stainless steels and nickel-base alloys in BWRs, to proceed primarily by a slip oxidation (dissolution) mechanism, which relates the propagation rate to the continual rupture of the protective oxide at the crack tip and the associated increase in oxidation rate in this region. This process (Figure A.19) has been successfully modeled in terms of key parameters such as crack tip strain rate (from applied/residual stresses), corrosion potential and conductivity (from surface chemistry/bulk water composition) and material composition/microstructure (e.g. degree of sensitization).

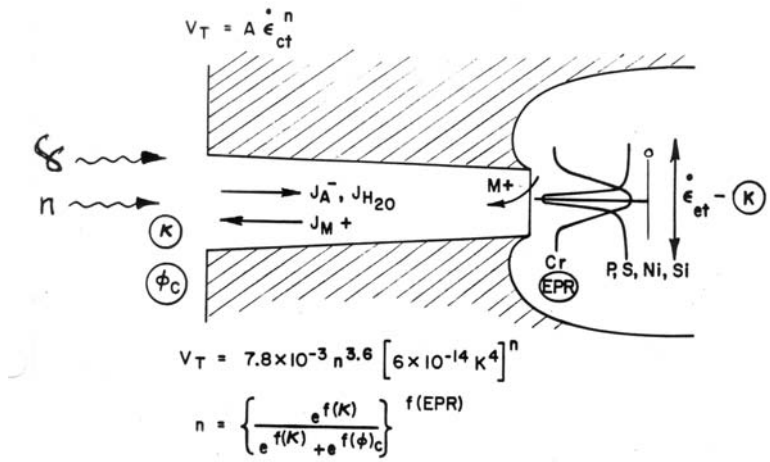

Figure A.19. Schematic of the crack enclave and the relevant phenomena associated with the slip oxidation mechanism of crack advance. Quantification of these phenomena has led to a lfe prediction methodology for austenitic stainless steels and nickel-base alloys in BWRs. [34, 35]

Mitigation of IGSCC is focused primarily on improved coolant chemistry (e.g. hydrogen water chemistry (HWC) and dissolved impurity reduction in BWRs, [see Appendix B.10] sometimes together with component surface modification (e.g. Noble Metal Chemical Addition (NMCA) or zirconia coating). However, stress reduction has also been used extensively (e.g. weld overlays for piping and clamps for internals in BWRs, improved tube support plate structures in PWR SGs, etc.). The primary emphasis has been on significantly reducing crack growth since minor intergranular attack (IGA) of austenitic alloys, which is a common initiating precursor, is often present from fabrication and/or cannot be prevented in operation. As indicated in Figure A.20, the knowledge of the quantitative understanding of the mechanism of crack propagation is able to predict the benefits of these mitigation actions, thereby offering assurance about successful future plant performance.

Key areas where further work is required include the effects of cold work (including locally in weld heat-affected zones) and the behavior of cast stainless steels and nickel-based weld metals, as well as the influence of specific, deleterious coolant impurities (e.g. lead, residues from ion-exchanger resins).

IGSCC of carbon and low alloy steels does not normally occur in LWR media [see Appendix B.8], but limited cracking of this type is known to have been observed in CANDU reactors and it should also be considered a possible degradation mechanism in concentrated boric acid environments, such as might form on external surfaces following leakage of PWR primary coolant.

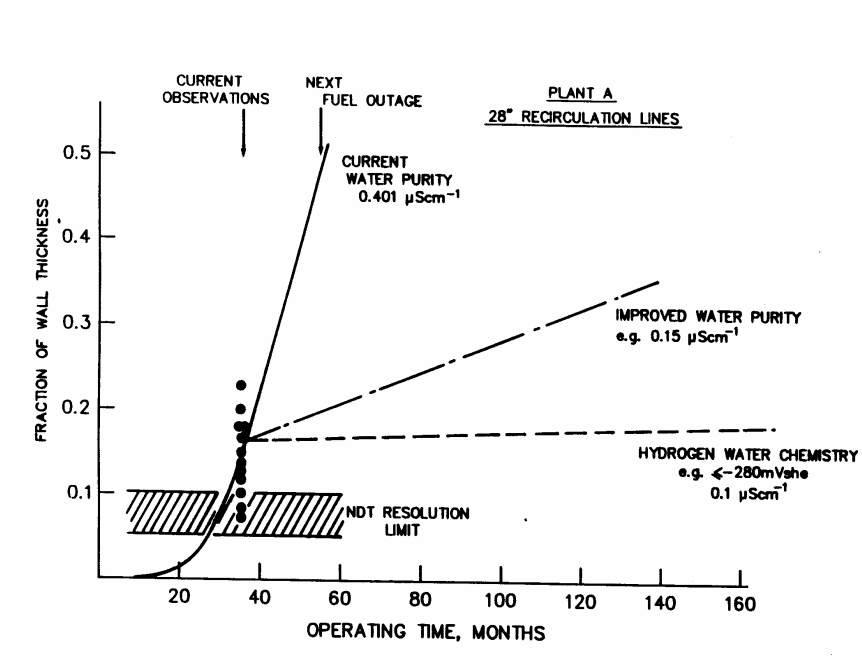

Figure A.20. Predicted response of defected piping for defined changes in water chemistry in BWR plant. [35]

Transgranular Stress Corrosion Cracking (TGSCC)

TGSCC may be observed in solution-annealed stainless steels since there is no metallurgical feature in the grain boundary akin to grain boundary chromium depletion in the sensitized condition to concentrate the corrosion processes in that region. In such cases the extent of cracking is governed by slip features that maintain a high oxide rupture rate at the crack tip, and environmental conditions such as the corrosion potential (or dissolved oxygen content) and aggressive impurities (e.g. chlorides) and oxidants that affect the chemistry at the crack tip (see earlier discussion on crevice chemistry). As would be expected from the discussion above on IGSCC it is possible to transition from IGSCC to TGSCC morphologies depending on the materials' degree of sensitization, slip characteristics (i.e. function of yield stress or degree of cold work) and dissolved oxygen/chloride content. An example of such transitions is shown in Figure A.21. It is apparent that TGSCC would not be expected to be a common phenomenon under normal BWR and PWR water chemistry regimes. However, as pointed out in the main report, such TGSCC incidences may become of importance for stainless steels, especially if the surface is highly cold worked, or on external component surfaces which may be contaminated with chloride deposits, or, in dead legs (e.g. for CRDMs and canopy seals in PWRs.) where impurities cannot be dispersed.

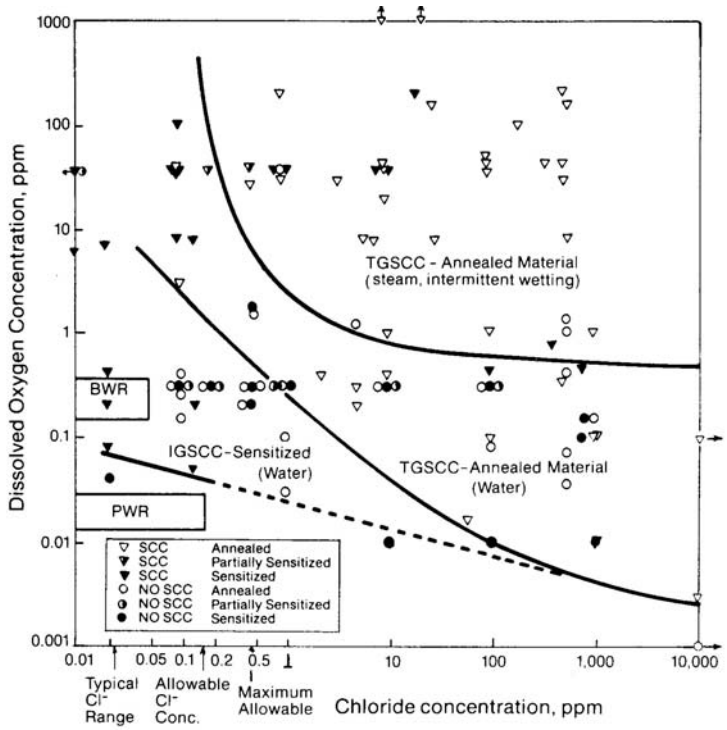

Figure A.21. Effect of oxygen and chloride concentration on the SCC of austenitic stainless steels in water 250-350oC, together with the oxygen/chloride ranges in BWR and PWR environments. [38]

Although carbon and low alloy steels are regarded as highly resistant to SCC under LWR conditions [see Appendix B.6], limited TGSCC has been observed, e.g. in SG shells exposed to faulted secondary water, and in BWR components subjected to high, local loads while operating with normal (oxygenated) water chemistry. Recent research suggests that occasional susceptibility may also be related to changes in the deformation behavior of particular steels associated with the dynamic strain aging that can occur at intermediate operating temperatures.

Primary Water Stress Corrosion Cracking (PWSCC)

PWSCC refers to intergranular cracking of any material, but particularly of Ni- base alloys such as Alloy 600 and its weld metals, in PWR primary coolant (i.e. containing lithium, boric acid and hydrogen) of correct nominal chemistry. Figure A.22 illustrates the main locations where PWRSCC has occurred [see Appendix B.6], whereas the schematic drawing in Figure A.23 illustrates the relationship between the shape of the axial crack in the Alloy 82/182 weld and Alloy 182 butter and the dissimilar metal low-alloy steel and stainless steel components.

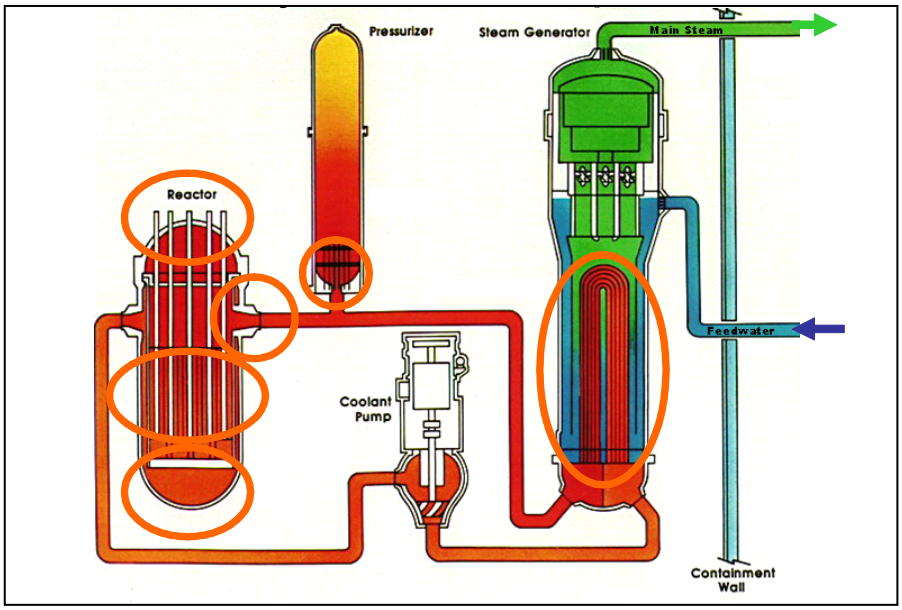

Figure A.22. Regions in the PWR Primary Reactor Coolant System where PWSCC of nickel base alloys have been observed.

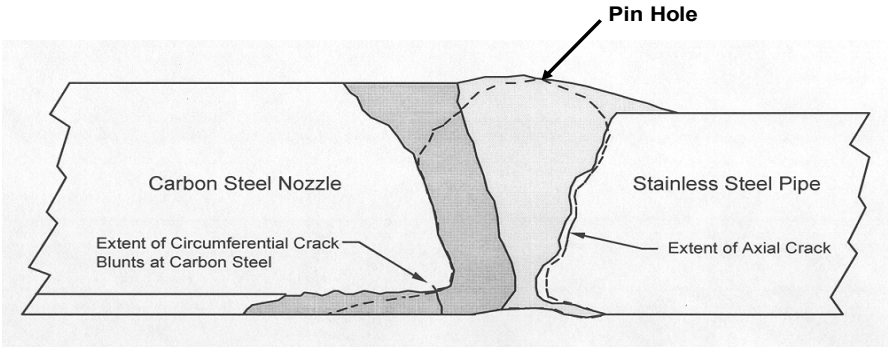

Figure A.23. Schematic diagram illustrating the locus of an axial PWSCC crack front in the Alloy 82/182 weld between dissimilar alloy carbon and stainless steel components. [ ]

Over the last thirty years, intergranular stress corrosion cracking in PWR primary water (PWSCC) has been observed in numerous components made of Alloy 600 and its associated weld metals (Alloys 82/182), sometimes after relatively long incubation times. In stark contrast to IGSCC of Ni-base alloys in other media (e.g. on the PWR secondary side) and to IASCC of these and other austenitic alloys, sensitization of the material through intergranular precipitation of chromium-containing carbides is beneficial to the PWSCC resistance of Alloy 600, which justifies its consideration in a separate category of cracking mechanism. However, large variations exist in the susceptibility of individual heats of material, even of nominally similar

composition and thermomechanical processing history, so that prediction of service behavior is difficult. Cold work is highly detrimental.

Cracking, which can also occur in pure hydrogenated water or steam, is highly temperature-dependent and appears to be associated with environmental conditions under which the surface films are in the transition region of Ni/NiO stability. Despite intensive research, there is no general agreement on the mechanism of PWSCC. Candidate theories include hydrogen assisted cracking, slip oxidation, thermally activated dislocation creep and internal oxidation. The latter has a particular attraction, since it could explain the very long times (>100,000 hours) sometimes necessary for cracking to initiate, even under conditions where subsequent crack propagation is relatively rapid. PWSCC of weld metals (and its possible interaction with fabrication defects such as hot cracking) is currently a high-profile topic that has been insufficiently studied and is not well understood.

To date, mitigation of PWSCC has usually involved repair and replacement actions using more resistant materials (such as Alloy 690). However, increased attention is now being paid to possible mitigation measures involving surface treatment (e.g. water-jet peening), chemistry optimization (e.g. adjustment of hydrogen levels and/or addition of potentially inhibiting species such as zinc), and various mechanical options to achieve a reduction in tensile stress levels.

Irradiation Assisted Stress Corrosion Cracking (IASCC)

The SCC behavior of irradiated stainless steels is a natural extension of IGSCC of un-irradiated stainless steel [see Appendix B.2], but the critical fluence level above which irradiation effects begin to dominate material behavior is complex. A lower value of ~$5x10^{20}$ n/cm^2 is often quoted for BWR internals, with saturation of the effects beginning at around $3x10^{21}$ n/cm^2, i.e. shortly before the expected end of life (EOL) fluence of ~$8x10^{21}$ n/cm^2. In contrast, IASCC in PWRs has only been observed (e.g. in baffle/former bolts) to start after reaching a fluence of ~$2x10^{21}$ n/cm^2 and little information is available about expected behavior near the much higher EOL fluence values typical of PWRs.

The mechanism of IASCC in PWR primary water is currently unclear, with no evidence that locally oxidizing conditions, grain boundary segregation, helium formation, or hydrogen embrittlement play a major role, although high strength from irradiation hardening does appear to be important (possibly analogous to the effects of cold work in SCC without irradiation). Mitigation measures are not yet available.

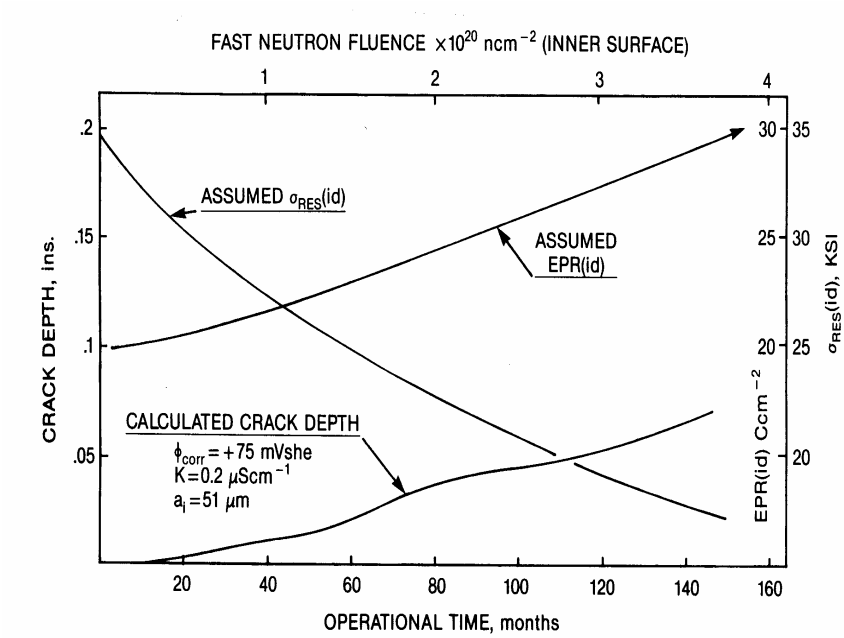

Figure A.24. Calculated change in crack depth in irradiated stainless steel as a function of fluence (e.g. time) due to specified changes in residual stress and degree of grain boundary sensitization. [ ]

Apart from its concurrent role in reducing fracture toughness, irradiation in BWRs is best viewed as an accelerant of many of the features shown schematically in Figure A.19. For instance, fast neutron irradiation increases the extent of grain boundary chromium depletion, it affects the crack tip strain rate through both irradiation induced hardening and relaxation of the residual stresses and, finally there is an elevation of corrosion potential. Such interacting irradiation effects affect the IASCC cracking kinetics in a, sometimes non-monotonic fashion, as illustrated in Figure A.24. Thus the mechanistic understanding of the roles that irradiation has on stress corrosion cracking of BWR core components and its relationship to the cracking that occurs in thermally sensitized microstructures, is relatively advanced [see Appendix B.2], and this has an impact on the judgments of the future IGSCC/IASCC performance of core components.

Mitigation of IASCC in BWRs is focused primarily on reductions in corrosion potential through the use of HWC/NMCA, i.e. an extension of the approach already taken for IGSCC, but the benefits are less well quantified.

Low-temperature crack propagation (LTCP)

LTCP refers both to high sub-critical crack growth rates (i.e., SCC, most likely from hydrogen assisted cracking) and to reduced fracture toughness [see Appendix B.13]. While the largest concerns are for higher strength Ni alloys (e.g., alloy X750 and alloy 182/82 weld metals), there are reasonable bases for concerns for base metals, particularly (but not only) if the yield strength is elevated (e.g., from cold work or irradiation).

Initial studies in the 1980s showed very rapid crack propagation in the temperature range 70-140°C in moderate to high strength Ni base alloys once IG SCC cracks had formed in high temperature water. The highest rates were observed in Alloy X750, although large effects were also observed for Alloy 182 and 82 weld metals and other Ni base alloys (e.g., aged Alloy 625, Alloy 718, and Alloy 690). The observations occurred in constant displacement (wedge/bolt loaded) specimens, in actively loaded specimens, and also in specimens exposed only to gaseous hydrogen in this temperature regime (leading to the reasonable conclusion that it's a hydrogen related phenomenon). More recently, it has been observed that significant reduction in fracture toughness (e.g., in J-R tests) can occur in the same temperature regime, under very specific loading rates.

The fact that these degradation effects are only observed when the specimens have been exposed to hydrogen (e.g. hydrogenated water) above a specific level strongly implies that the mechanism of both embrittlement and increased subcritical crack propagation is related to hydrogen embrittlement. However, the exact mechanism is unknown, and the conjunction between the PWR plant operations and the observed requirements of temperature, alloy content and microstructure, and strain rate for these degradation phenomena to become significant, is the object of high priority studies.

A.4.3 Fatigue

This section addresses materials degradation due to fatigue, an aging degradation mechanism that can affect a number of major components throughout the primary pressure boundary of both PWRs and BWRs. [see Appendix B.14]. Components that may be affected range from the low alloy steel reactor pressure vessel, pressurizer and steam generator shell to stainless steel pumps, piping etc. to nickel base alloy welds, tubing etc. This degradation mode is an extremely well researched topic, fatigue being, unlike many of the other degradation modes, considered in the original reactor design basis.

From a categorization viewpoint, fatigue may be regarded in terms of “High Cycle Fatigue”, “Low Cycle Fatigue”, “Thermal Fatigue” and “Environmental (or Corrosion) Fatigue”. Superimposed upon these categorizations is the (sometimes semantic) division of degradation periods between “initiation” and “propagation”. Some of these categorizations and environmental impacts may be understood in relationship to Figures A.25 (a) and (b). At the reactor design stage the fatigue life, which forms part of the design basis, is calculated from a strain-amplitude vs crack initiation time (or cycles) database that corresponds to the curves in Figures A.25a and A.25b marked “air”. These curves (in this example for carbon steel) are based on data obtained in air at 25°C for smooth cylindrical specimens, cyclically loaded under strain control; “initiation” in this case is defined as a drop in maximum load by 25%, which physically corresponds to a crack of 1-2 mm depth.

The categorization of “high-cycle fatigue” refers to a high number of cycles at a relatively low stress amplitude (typically below the material’s yield strength but above the fatigue endurance limit of the material), with the driving force for the cyclic loading coming from, for instance, flow induced vibrations and/or instabilities in thermal mixing of the coolant. On the other hand ”low-cycle fatigue” refers to the higher stress/strain amplitude regime, where the local yield

stress may be exceeded leading to correspondingly shorter fatigue lives; such a regime is associated with, for instance, lower frequency operational transients (such as plant start-up/shut-down or hot stand-by). "Thermal fatigue" is due to cyclic stresses/strains that result due to changing temperature conditions in a component or in the piping attached to the component. Thermal fatigue may involve a relatively low number of cycles at a higher stress (e.g., plant operational cycles or injection of cold water into a hot nozzle) or due to a high number of cycles at low stress amplitude (e.g. local leakage effects or cyclic stratification).

Design against fatigue damage is based primarily on the fatigue curves in Section III, Appendix I (e.g., Figures I-9.1 and I-9.2) of the ASME Code. In this design process, the fatigue cycles are decreased from those denoted by the "air" data lines in Figure A.25, in order to take into account unknown effects of temperature, surface roughness, environment, etc. The extent of this decrease is based on engineering judgment and, as indicated in Figure A.25b, the "design curve" is displaced from the data curve by a factor of two (on stress/strain amplitude) or 20 (on fatigue life), whichever was the more conservative. It is this design curve that the fatigue "Cumulative Usage Factors" (CUF) are calculated for decisions on continued reactor operation. As discussed in Appendix B.14, there is much discussion internationally about the appropriateness of this "2 and 20" design line, especially when environmental effects need to be accounted for [39-41].

This concern for the effect of the environment on crack initiation (and ultimately for long crack propagation) is discussed in Appendix B.14, but the essence is illustrated in Figure A.25 for the specific case of carbon steel in LWR environments. It has been demonstrated in several studies that the decrease in the fatigue life below that observed in dry air is a function of the strain rate applied during the loading period, hold time (in a trapezoidal loading scheme), corrosion potential, temperature, minimum/maximum strain ratio, water purity. To a large extent these dependencies are predictable via the knowledge of the environmentally assisted cracking mechanisms discussed earlier [42]. Moreover similar dependencies are observed for most of the ferritic and austenitic alloys in LWRs and as indicated in Figure A.25 (b) for carbon steel piping there are combinations of these system parameters that lead to fatigue lives that are less than the currently accepted design values.

As also discussed in Appendix B.14, there are similar concerns about the effect of the environment on the fatigue crack propagation rates that are used for crack disposition decisions according to ASME XI procedures. In this case significant progress has been made, however, for the specific case of LAS in PWR reactor water through the introduction of Code Case N-643 [45], which is currently undergoing further refinement.

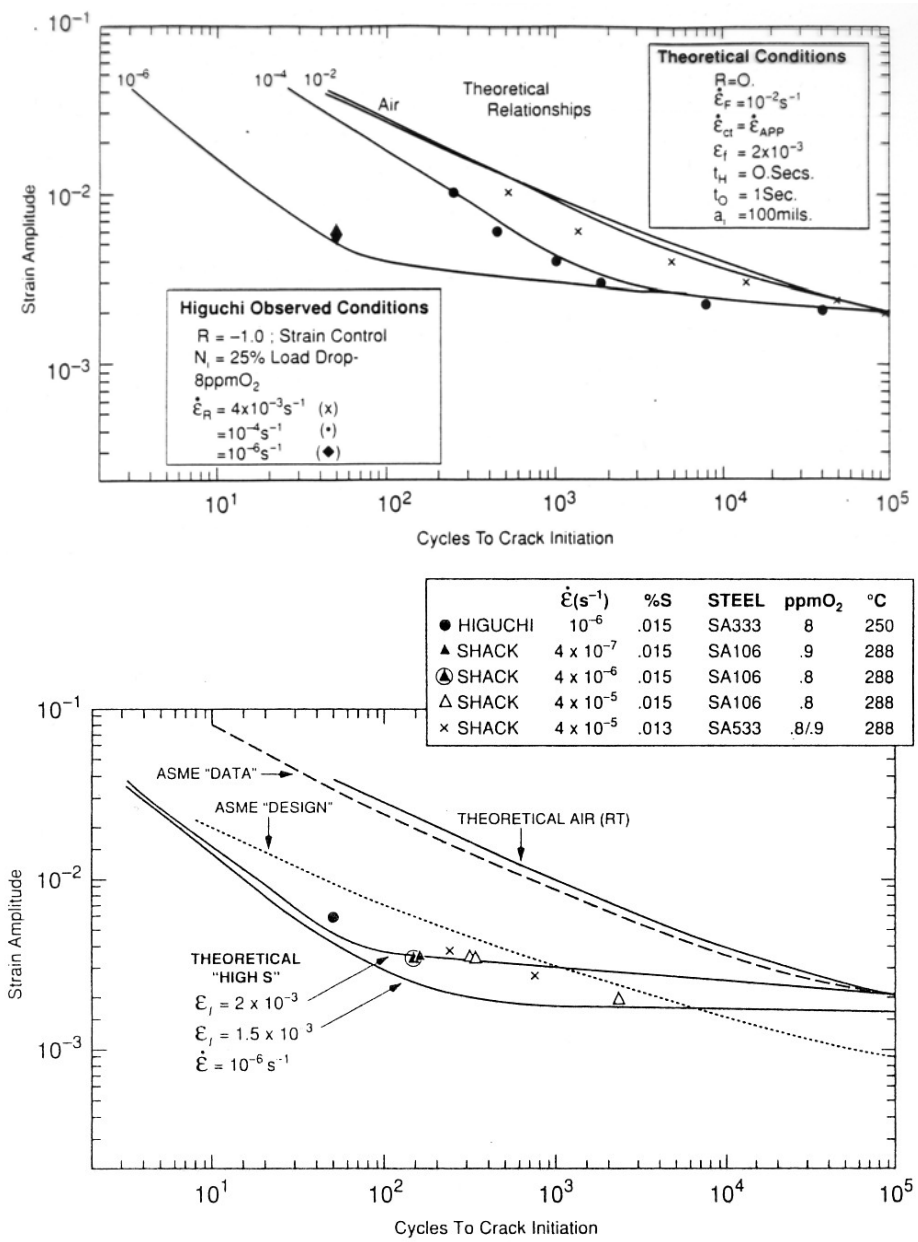

Figure A.25. (a) Predicted [42] and observed [43] strain amplitude versus cycles to crack initiation relationships for unnotched carbon steel in 288°C, 8 ppm oxygenated water with strain applied at different rates. (b) Predicted [42] and observed [43, 44] strain amplitude versus cycles to crack initiation relationships for unnotched carbon and low alloy steels in 288°C water, under the worst combination of material and environmental conditions. Note the non-conservatism of the ASME III design curve under these conditions at certain strain amplitudes

A.4.4 Loss of Fracture Resistance

This section addresses material degradation mechanisms that lead to a reduction in the fracture toughness of the material with increasing time. Because a high level of fracture toughness is a design assumption for most LWR pressure boundary and internal components, degradation mechanisms that lead to reductions of toughness are of high significance for many components.

Two distinct degradation mechanisms are addressed in this section, radiation embrittlement and thermal aging. A third loss of fracture resistance issue, associated with some nickel base alloys after having been exposed to hydrogenated water, and tested at specific loading rates in a specific temperature range was discussed previously in this Appendix, and this is discussed in more detail in Appendix B.13.

Many of the materials of LWR construction are potentially sensitive to thermal aging or neutron embrittlement and in some cases arguments have been made for synergistic effects between the two degradation modes. An example of this, identified by the NRC in Safety Evaluation Reports, would be cast austenitic alloys in PWRs. To date, however, no data have been presented to prove or disprove the existence of such synergistic effects.

Neutron Embrittlement

Radiation embrittlement results in an increase in the material's yield and ultimate strengths, with a corresponding decrease in material ductility and resistance to flaw propagation (fracture toughness). Radiation embrittlement in ferritic steels is measured by an increase in the ductile-to-brittle transition temperature (RT_{NDT}) and a drop in the Charpy upper shelf energy. Embrittlement in ferritic steels is primarily caused by the formation of copper-rich precipitates that harden the matrix and reduce toughness. Neutron irradiation enhances the formation of these precipitates.

Extensive databases exist for evaluating and predicting embrittlement in reactor vessel steels. These data are obtained from vessel material surveillance capsules in both PWR and BWR vessels, and from test reactors. Embrittlement trend curve models such as Regulatory Guide 1.99, Rev. 2 are used to predict the shift in RT_{NDT} and drop in upper shelf energy as a function of copper, nickel, and fluence.

Significant variations in radiation embrittlement have also been observed between different types of steel (carbon and low alloy steels, etc.) and even between different heats of the same steel. These differences are caused by variations in metallurgical structure and composition. Improved empirical trend models have recently been developed to describe the combined effects of copper, nickel, phosphorus, irradiation temperature, and neutron flux and fluence on the embrittlement of pressure vessel steels. Steels with a very low copper content show little embrittlement in spite of high radiation doses. The effect of irradiation exposure at low temperatures (below 525°F) increases the rate of embrittlement damage. Weld metal is generally more sensitive to radiation embrittlement than base metal. Impurity chemistry, chemistry variability, and different microstructure are responsible for the greater sensitivity of the weld metal. In 2002 this improved trend curve model was approved in a revision to ASTM Standard Guide E900.

Stainless steels are also affected by irradiation exposure [see Appendix B.2], but do not exhibit a ductile-to-brittle transition. In stainless steels, reduction in the ductile fracture toughness properties is associated with microstructure changes resulting from the effects of neutron interactions. Neutrons interact with atoms in the crystal lattice, both directly and indirectly, to displace atoms in the lattice and alter material properties through formation of dislocations, interstitials, and vacancies. Segregation of material impurities also occurs.

Data are available from austenitic stainless steel components exposed to neutron irradiation in experimental and thermal reactors. They show that significant reductions in material J-integral values and tearing modulus values appear at approximately one displacement per atom (dpa). Reductions in these fracture toughness properties appear to saturate at fast neutron exposures greater than 10 dpa.

Currently, there is a lack of substantive fracture toughness data for austenitic stainless steels exposed to a neutron fluence exceeding $\sim 10^{21}$ n/cm^2 in an LWR environment. The bulk of existing data are developed from materials irradiated in experimental reactors. Differences in neutron spectra of experimental reactors and light water reactors could result in actual material property changes. Specific data regarding irradiation exposure of cast stainless steels in an LWR environment are particularly limited.

Void Swelling Effects

Void formation is a mechanism in which radiation-induced vacancies accumulate in metal to form microscopic voids. If a large number of voids form, termed void swelling, dimensional changes can occur and loads at connection points (for example, at bolted or welded joints of structural members) may also be altered. Thus void swelling could potentially affect the intended functionality of certain component(s). Based on available fast-reactor data, significant fracture toughness reduction of SS materials can also occur if void swelling is large (i.e., greater than several percent).

Thermal Aging

Thermal aging [64] has been shown to cause precipitation of additional phases in the ferrite such as formation of an α phase by spinoidal decomposition, nucleation and growth of an α phase, or nucleation and growth of carbides at the ferrite/austenite phase boundaries. Development of these additional phases results in an increase in hardness and yield strength of the casting, with a corresponding reduction in fracture toughness properties. As a result, the component becomes more susceptible to brittle fracture when sufficient tensile loadings are present to drive crack growth. A brittle fracture occurs when the ferrite phase becomes continuous or the ferrite/austenite phase boundary provides an easy path for crack propagation in the presence of an existing flaw and sufficient stresses. This type of failure is due to cleavage of the ferrite or separation of the ferrite/austenite boundary and is termed “channel fracture.”

The effects of thermal aging on casting fracture toughness have been shown to saturate once conditions leading to predominantly brittle fracture occur. This saturation effect is associated with development of channel fracture conditions. While the extent of reductions in casting

fracture toughness due to thermal aging is related to operating temperature, time at temperature, casting method (static vs. centrifugal), and material composition (molybdenum and ferrite content), available research results indicate that the saturation fracture toughness (Cvsat) can be correlated to casting chemical composition, material properties and the casting method. The actual casting toughness decreases logarithmically with increased operating time toward this "infinite-time" saturation value so the use of Cvsat as a measure of casting fracture toughness is conservative.

Thermal aging embrittlement of materials other than CASS used in reactor components includes (1) temper embrittlement and (2) strain aging embrittlement. Ferritic and low alloy steels are subject to both of these degradation mechanisms but wrought stainless steels are not affected by either mechanism.

Temper embrittlement of low alloy steels is caused by the diffusion and segregation of impurity elements, such as phosphorous, tin, antimony and arsenic, into the grain boundaries after prolonged exposure to temperatures in the range 662°F (350°C) to 1067°F (575°C). At temperatures above this range, the impurities tend toward solution in the ferrite matrix. For example, little or no grain boundary segregation is observed at temperatures above 1157°F (625°C). At temperatures below this range, very long exposure times are necessary for the impurities to diffuse to, and segregate in, the grain boundaries. The presence of carbon tends to accelerate the embrittlement process, due to preferential segregation of the impurities at the interface between grain boundary carbides and ferrite grains. The role of other alloying elements, such as chromium, nickel, magnesium, and molybdenum, in the acceleration or retardation of the temper embrittlement process has been studied extensively. The principal manifestation of temper embrittlement in low alloy steels is an increase in ductile-to-brittle transition temperature, due to the change from predominantly cleavage fracture (before temper embrittlement) to predominantly intergranular fracture along impurity segregation paths (after temper embrittlement).

Strain aging embrittlement occurs in cold worked ferritic steels when they are subjected to temperatures in the range of 500-700°F, and is caused by the pinning of dislocations by interstitial impurities (nitrogen, carbon, etc.). Post-weld heat treatment of reactor vessel components following cold working during fabrication mitigates, but does not eliminate, the effects of strain aging embrittlement. However, following post-weld beat treatment, residual strain aging embrittlement has only a slight effect on the ductility and fracture toughness of LWR vessel component materials under the environmental and loading conditions of interest.

A.5 References

[1] "Corrosion", Vol. 13, Metals Handbook, ASM International, 1987.

[2] "Uhlig's Corrosion Handbook," Ed R.W. Revie, J.Wiley and Sons Inc, 2nd Edition, 2000.

[3] "Corrosion," Ed. L.L.Shrier, R.A.Jarman & G.T.Burstein, Butterworth-Heinemann Ltd, 3rd Edition, 1994.

[4] D. A. Jones, "Principles and Prevention of Corrosion," Prentice Hall, 2nd Edition, 1996.

[5] D.D Macdonald & G.A.Cragnolino, "Corrosion of Steam Cycle Materials," Chapter 9 in "The ASME Handbook on Water Technology for Thermal Power Systems," Ed. Paul Cohen, Pub. ASME, 1989.

[6] M.G. Fontana, "Corrosion Engineering," Pub McGraw Hill, New York, 3rd Edition, 1986.

[7] M. Pourbaix, "Atlas of Electrochemical Equilibria in Aqueous Solutions," Ed. NACE, 1974.

[8] Z. Szklarska-Smialowska, "Pitting Corrosion of Metals," Pub NACE, 1986.

[9] G.M.W. Mann, "History and Causes of on-Load Waterside Corrosion," Br. Corrosion Journal, 1, pp6-14, 1977.

[10] B.M. Gordon, R.L.Cowan, C.W.Jewett and A.E. Pickett, "Mitigation of Stress Corrosion Cracking through Suppression of Radiolytic Oxygen," Proceedings of First International Symposium on Environmental Degradation in Nuclear Power Systems – Water Reactors. Myrtle Beach August 22-25, 1983. Eds. J.Roberts, W Berry. Published by National Association of Corrosion Engineers. ISBN 0-915567-00-8. pp. 893–932.

[11] S. Hettiarachchi, "NobleChem from Concept to Operating Commercial Power Plant Application." Proceedings of Tenth International Conference on Environmental Degradation in Nuclear Power Systems – Water Reactors. Lake Tahoe, August 5-9, 2001. Eds. F.P.Ford, G.Was. Published by National Association of Corrosion Engineers.

[12] E.G.Brush, W.L.Pearl, "Corrosion and Corrosion Product Release in Neutral Feedwater," Corrosion, 28, 4, pp. 129-136, 1972.

[13] R.K. Freier, "Operating Experiences with Protective Layers of Metal Oxides, Using Addition of Oxygen," Vom Wasser, 38, Ed. Verlag Chemie Gmbh, Weinheim, Bergstr., 1971.

[14] "Boric Acid Corrosion of Carbon Steel Reactor Pressure Boundary Components in PWR Plants," NRC Generic letter 88-05, March 17, 1988.

[15] "Boric Acid Corrosion Guidebook." EPRI Report 1000975, 2001.

[16] L.Tomlinson, "Mechanism of Corrosion of Carbon and Low Alloy Steels by High Temperature Water," Corrosion, 37, pp. 591-596, 1981.

[17] C.Czajkowski, "Metallurgical Evaluation of an 18 inch Feedwater Line Failure at the Surry Unit 2 Power Station," NUREG/CR-4868, Brookhaven Nat. Lab., March 1987.

[18] B.Chexal, et. al., "Flow Accelerated Corrosion in Power Plants," EPRI Report TR-106611, June 1996.

[19] "CHECWORKS TM Computer Program Users Guide." EPRI Report TR103198-P, June 1998.

[20] G.J.Bignold, K.Garbett and I.S Woolsey, "Mechanistic Aspects of the Temperature Dependence of Erosion – Corrosion," Proceedings of Conference "Corrosion Erosion of Steels in High Temperature Water and Wet Steam," May 1982, Eds. Ph Berge, F.Kahn. Pub. Electricitie de France.

[21] Conference on "Localized Corrosion," Dec 6-10, 1971, Williamsburg, Ed. B.F.Brown, J.Kruger, R.W.Staehle, Pub NACE 1974.

[22] "Localized Corrosion-Cause of Metal Failure," ASTM STP 516 1972.

[23] R.W.Staehle, "Bases for Predicting the Earliest Penetrations due to Stress Corrosion Cracking for Alloy 600 on the Secondary Side of PWR Steam Generators," US NRC Report NUREG/CR-6737, 2001.

[24] Kolotyrkin,Ya. M., "Pitting Corrosion of Metals," Corrosion,19, 8, pp. 261t-268t, 1963.

[25] Z. Szklarska-Smialowska, "Review of Literature on Pitting Corrosion Published since 1960," Corrosion, 27, pp.223-233, 1971.

[26] M.Karaminezhaad-Ranjbar, J.Mankowski, and D.D Macdonald, "Pitting Corrosion of Inconel 600 in High Temperature Chloride Solution under Controlled Hydrodynamic Conditions," Corrosion, 41,4, pp.197-204, 1985.

[27] J.R.Park, Z. Skaklarska-Smialowska, "Pittong Corrosion of Inconel 600 in High Temperature Water Containing $CuCl_2$," Corrosion, 41,11, pp.665-675, 1985.

[28] T.Shibata, and H.Takamiya, "Effect of pH and Cl^- on the Stochastic Process of Pitting Corrosion of Mo Containing Stainless Steels," in Proceedings of *"Critical Issues in Reducing the Corrosion of Steels,"* Ed. H.Leidheiser and S.Haruyama. USA-Japan Seminar Nillo Japan, 1985.

[29] T.Shibata and T.Takeyama, "Stochastic Theory of Pitting Corrosion," Corrosion, 33,243, 1977.

[30] D.D Macdonald and M. Urquidi-Macdonald, "Distribution Functions for the Initiation of Pitting Attack on Passive Alloys," Ind. J. Technology, 24,485, 1986.

[31] D.D Macdonald and M. Urquidi-Macdonald, "Distribution Functions for the Breakdown of Passive Films," Electrochimica Acta, 31, 1079, 1987.

[32] J.A.Beavers et. al., "Corrosion Related Failures in Power Plant Generators," EPRI Report NP-1468, 1980.

[33] R.W.Staehle and B.J.Little, "Corrosion and Stress Corrosion Cracking of Post Tension Cables Associated with Funfal Action," Corrosion, 2002, April 7-11, 2002.

[34] F.P. Ford, D.F. Taylor, P.L. Andresen and R.G. Ballinger, "Corrosion-Assisted Cracking of Stainless Steel & Low-Alloy Steels in LWR Environments," Report NP5064S, (February 1987), EPRI, Palo Alto.

[35] F.P.Ford, "The Crack Tip System & it's Relevance to the Prediction of Cracking in Aqueous Environments" Proceedings of First International Conference on Environmentally Assisted Cracking of Metals, Kohler Wisconsin October 2-7 1988. Pp.139-165. Eds. R.Gangloff & B.Ives, Pub. NACE.

[36] M.O.Speidel, "Stress Corrosion Cracking and Corrosion Fatigue-Fracture Mechanics," in *"Corrosion in Power Generating Equipment,"* Eds, M.O. Speidel, A.Atrens, Pub. Plenum Press, NY. 1984.

[37] B.M.Gordon & G.M.Gordon,"Corrosion in Boiling Water Reactors." ASM Handbook Corrosion Vol 13. 1987, pp929, 937.

[38] B.M.Gordon, "The Effect of Chloride and Oxygen on the Stress Corrosion Cracking of Stainless Steels; Review of Literature," Materials Performance, 19, pp.29-38, 1980.

[39] NUREG/CR-6583 (ANL-97/18), "Effects of LWR Coolant Environments on Fatigue Design Curves of Carbon and Low-Alloy Steels," March 1998.

[40] NUREG/CR-5704 (ANL-98/31), "Effects of LWR Coolant Environments on Fatigue Design Curves of Austenitic Stainless Steels," April 1999.

[41] NUREG/CR-6674 (PNNL-13227), "Fatigue Analysis of Components for 60-Year Plant Life," June 2000.

[42] F.P.Ford, "Prediction of Corrosion Fatigue Initiation in Low Alloy Steel and Carbon Steel/Water Systems at 288°C", Proceedings of Sixth International Symposium on Environmental Degradation in Nuclear Power Systems – Water Reactors. San Diego, August 1-5, 1993. Eds. E Simonen, R. Gold, Published by National Association of Corrosion Engineers. ISBN 0-915567-00-8. pp.9-16.

[43] M. Higuchi and K.Iida, Nuclear Engineering and Design, 129, pp293-306, 1991.

[44] W.Shack et. al., "Environmentally Assisted Cracking in LWRs," NUREG/CR 4667, vol.14, 1992.

[45] ASME Code Case-643, "Fatigue Crack Growth Rate Curves for Ferritic Steels in PWR Water Environment," May, 2000.